STAGGERED TIME INTEGRATION METHODS FOR A ONE-DIMENSIONAL EULER AEROELASTIC PROBLEM

Serge Piperno
CERMICS
INRIA, B.P. 93, 06902 Sophia-Antipolis Cedex, France.

Abstract

In this paper, we consider two one-dimensional aeroelastic model problems. We investigate stability characteristics of staggered procedures of time-integration for these coupled systems. The modularity of these staggered schemes allows the use of classical upwind schemes for the fluid part of the problem (possibly subcycled explicit scheme) and Newmark or generalized-α methods for the structure. Though these methods have well known decoupled stability limits, the stability of the coupled scheme for a non-linear problem is unknown. We first present the volume-continuous method and we show this very popular algorithm produces a violation of action-reaction principle at the fluid/structure interface. This default is corrected in the new volume-discontinuous method, which is shown to have enhanced flexibility and stability properties. Finally, the extension possibilities of this new method to multi-dimensional cases are discussed.

METHODES D'INTEGRATION TEMPORELLE DECALEE POUR UN PROBLEME AEROELASTIQUE MONO-DIMENSIONNEL NON LINEAIRE

Résumé

Dans ce rapport, nous présentons deux problèmes modèles aéroélastiques. Nous étudions la stabilité de méthodes d'intégration temporelle décalée pour ces problèmes couplés. Leur modularité permet l'emploi de schémas décentrés explicites (éventuellement sous-cyclés) pour le fluide et implicites pour la structure dont les stabilités découplées sont connues. Cependant, la stabilité du schéma couplé reste inconnue. Nous présentons d'abord la méthode avec interface simple. Nous montrons que cette méthode très populaire viole le principe d'action et de réaction à l'interface fluide/structure. Ce défaut est corrigé dans la nouvelle méthode avec interface double. Nous montrons que cette dernière est plus souple et plus stable. Pour finir, l'extension de cette nouvelle méthode à des cas multi-dimensionnels est envisagée.

1 Introduction

We present in this paper some numerical methods that have been constructed for the numerical simulation of fluid-structure interactions. This class of coupled problems and some classical methods used for their simulations have been reviewed in previous works [1]. Shortly, numerical methods used for the simulation of aeroelastic problems should have the following qualities: accuracy, efficiency and modularity. The accuracy of the methods used allows the interpretation of numerical results, which are the sum of the exact solution of the modelized problem and the numerical errors (numerical damping and diffusion, dispersion). For example, the Euler flutter analysis of an airfoil [2] can be done if the numerical diffusion does not make flutter disappear. Efficiency allows accurate computations with limited costs. In some cases, the characteristic times of the fluid part and the structural part of the coupled system are very different. Their time-integrations might require very different time steps. Efficiency can be enhanced with the use of subcycling [3]. Finaly, by the use of staggered schemes [4], modularity is achieved. Most popular existing modules for the separate resolutions of fluid and structural parts can be coupled. Each part can be dealt with separately, and even computed on separate heterogeneous machines [3]. As a consequence, some particular coupling methods are required.

The aim of this paper is to present some numerical methods constructed for the numerical simulation of a one-dimensional Euler aeroelastic model problem. Though the problem is very simple, we intend to only consider methods that could be extended to multidimensional, complex cases. This paper follows a preceding study on the linearization of the same model problem [5], and some proved stability results on numerical methods used for the simulation of linear aeroelastic problems [3].

The content of this report is as follows. In Section 2, we present the aeroelastic problems considered. These two very similar problems are one-dimensional. The structure is linear with a single degree of freedom. The fluid satisfies 1D Euler equations (perfect fluid). They differ by some boundary conditions for the fluid. These problems were chosen because they are simple, and have the same characteristics as some other aeroelastic problems: the piston problem is mainly internal and acoustic, while the box problem is rather external (close to the flutter case analyzed in [6, 2]).

In Section 3, we present the global resolution algorithm. We use staggered schemes, which allow modularity. We then have to present the set of numerical methods used separately in the fluid (finite volume method, Van Leer flux splitting) and the structural (generalized-α method) part of the problem. We also present the methodology for the coupling of the previous methods, and the necessity of subcycling.

In Sections 4, we show and analyze the volume-continuous method, which is currently used in industrial codes. Both fluid and structural mesh boundaries are matching (at least the continuous interfaces are matching before separate spatial discretizations). We explain why this method does not respect the action/reaction principle (and the conservation of the momentum), which might be the cause of its poor subcycling stability properties.

In Section 5, we present the volume-discontinuous method. The boundaries of the fluid and structural meshes are different. We show that this method allows the conservation of the momentum. The flexibility of the method is used with multiple prediction algorithms, in order to enhance the stability and the accuracy of the method.

Finally, we discuss in Section 6 the use of more complex time-interpolation schemes, and the possibilities of extension to multi-dimensional cases.

2 The model problems

In this section, we set the physical problems which will be studied in this paper. These two problems were needed because of their different relations with well-known aeroelastic test-cases. In the following, we first present the model problems. Then we set the corresponding mathematical problems. Finally, we explain our choice, based on eigenfrequencies considerations and similarities with cases of external flows and flows with strong compressibility effects.

2.1 The two one-dimensional problems

In this paper, we consider two one-dimensional problems which are quite close indeed. The first one, which will be called the "piston" problem, is shown on Figure 1. A perfect gas flow is contained in a chamber closed by a moving piston. The other end of the chamber is fixed. The structural part of this problem - the piston - closes the fluid domain, which produces the fluid/structure interaction. The problem will be set in more details in the following.

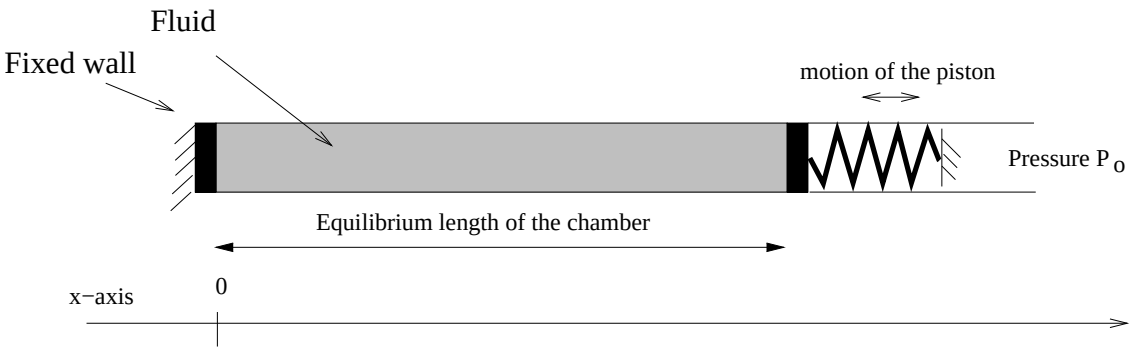

Figure 1: The "piston" problem (fluid-filled 1D flexible chamber with one moving end)

The second problem we will consider is shown on Figure 2. In the "box" problem, both ends of the chamber are moving. However, the length of the box remains constant (both ends speeds are equal). Again, there is an interaction between the fluid and the box - the structural part of the problem - because the box contains the fluid, which reciprocally exerts a pressure force at both ends.

In both problems, we assume no point of the flow is transonic and structural speeds are small compared to the average fluid sound speed. We will denote by X the displacement of the right end of the chamber. We will write x_L and x_R for the abscissae of the left and right ends. The origin of the X-axis is set at the left end of the chamber. The equilibrium length of the chamber for the piston problem is set to L, which also is the fixed length of the box in the box problem. We have $x_R = L + X$ and $x_L = 0$ (resp. $x_L = X$) for the piston (resp. box) problem. We assume the one-dimensional flow inside the chamber is governed by the compressible Euler equations. In both cases, we will refer to the equilibrium state of the system as the state where:

- the flow is uniform, with no velocity. The pressure is equal to the external pressure P_0
- the right end has no speed, and is at the equilibrium position.

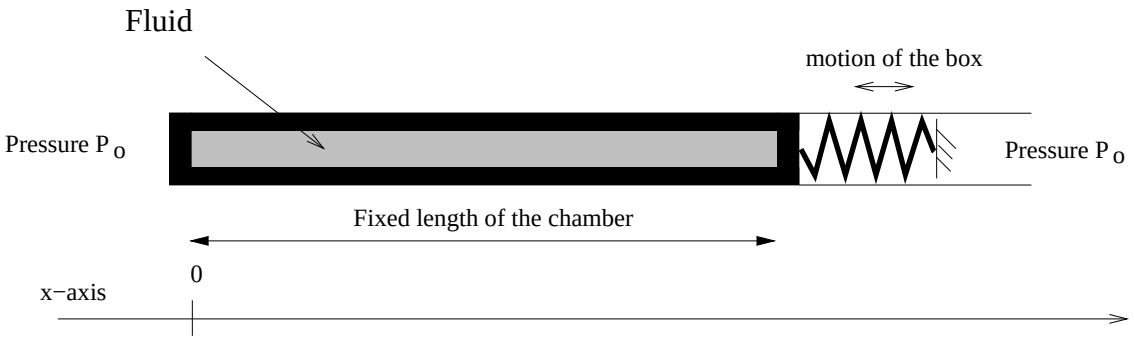

Figure 2: The "box" problem (rigid fluid-filled 1D moving box)

These problems have different characteristics. In the piston problem, the length of the chamber is variable. Then strong compressibility effects occur. The behaviour of the flow is close to a very rigid spring. As a matter of fact, this case is not far from an internal fluid/structure interaction problem. Paradoxally, the problem of the box is close to an external flow case. The fluid is not globally compressed since the length of the box is fixed. The fluid is just displaced, like the flow around an airfoil in subsonic flight. These aspects will be verified by the determination of first acoustic coupled eigenfrequencies.

2.2 Equations and boundary conditions

Mathematically, the problem is the following:

- Euler equations for the fluid in the domain $[x_L; x_R]$

$$\left\{ \begin{array}{l} \rho_t + (\rho u)_x = 0 \ , \\ (\rho u)_t + (\rho u^2 + P)_x = 0 \ , \\ E_t + [u(E+P)]_x = 0 \ . \end{array} \right. \tag{1}$$

  Here, ρ is the density, u is the velocity, P is the pressure and E is the total energy per unit volume. The fluid is assumed to be perfect and the pressure is given by

$$P = (\gamma - 1)(E - \frac{1}{2}\rho u^2) \tag{2}$$

  where γ is set to 1.4.

- boundary conditions for the fluid are the following:

$$\left| \begin{array}{rcl} u(x_L) & = & \dot{x_L} \\ u(x_R) & = & \dot{x_R} \end{array} \right. \tag{3}$$

  where dotted variables stand for corresponding time derivatives. They reduce to

$$\begin{array}{ll} \text{Piston problem:} & \left\{ \begin{array}{rcl} u(0) & = & 0 \\ u(L+X) & = & \dot{X} \end{array} \right. \\ \text{Box problem:} & \left\{ \begin{array}{rcl} u(X) & = & \dot{X} \\ u(L+X) & = & \dot{X} \end{array} \right. \end{array} \tag{4}$$

- the motion of the structure is given by

$$m\ddot{X} + d\dot{X} + kX = F \tag{5}$$

where m, d and k are respectively the mass, the internal damping and the stiffness of the structure. The external force F is given by

$$\begin{array}{rl} \text{piston problem:} & F = P(x_R) - P_0 = P(L+X) - P_0 \\ \text{box problem:} & F = [P(x_R) - P_0] - [P(x_L) - P_0] = P(L+X) - P(X) \end{array} \tag{6}$$

2.3 Coupled eigenfrequencies

We are interested in the numerical simulation of the two problems we just set. In both cases, the unique source of energy dissipation is the damping in the structural part. Then, we control the damping of the coupled system. For example, if we choose $d = 0$, we know that some global energy is conserved. Like aircraft conceptors, we would like to know the discrepancies between numerical simulations and physical experiments in the stability measured for the coupled system. In our cases, we will just have to test if our numerical results are rather stable or unstable, and to know what damping or amplification rates are numerically produced. We will also be interested in phase errors, and we need an estimation of the coupled frequencies of our problem.

In this paper, we will only consider small perturbations of the equilibrium states defined previously. Thus we intend to perform a linear stability analysis around these equilibrium states. We will use linearizations of our equations around these equilibrium states to obtain coupled eigenfrequencies of the problems. However, we will solve non-linearized problems with classical non-linear methods.

The linear stability analysis around equilibrium states can be found in details in [5]. We give here a sketch of main parts of these analyses.

In the following, ρ_0 is the uniform density at equilibrium and c is the sound speed (given by $\gamma P_0 = \rho_0 c^2$). We add a perturbation to all variables: a density perturbation $\Delta\rho$ ($\Delta\rho \ll \rho_0$), a velocity perturbation Δu ($\Delta u \ll c$). The pressure perturbation is given by

$$\Delta P = c^2 \Delta\rho \ , \tag{7}$$

which is derived from the isentropic hypothesis we make. Finally, the energy perturbation can be derived from the other perturbations. More, the linerization of the energy conservation equation (third Euler equation) reduces to an equation which is always verified (when the linearized forms of mass and momentum conservation equations are verified). Then, we get rid of this equation under the isentropic hypothesis.

Using the notation $W = (\Delta\rho, \rho_0 \Delta u)^t$, both problems reduces to the following:

- acoustic fluid equations written

$$W_t + \begin{pmatrix} 0 & 1 \\ c^2 & 0 \end{pmatrix} W_x = 0, \text{ on } [0; L] \text{ for both problem,} \tag{8}$$

- with boundary conditions given by

$$\begin{array}{rl} \text{piston problem:} & \Delta u(0) = 0 \text{ and } \Delta u(L) = \dot{X} \\ \text{box problem:} & \Delta u(0) = \Delta u(L) = \dot{X} \end{array} \tag{9}$$

- a structural equation which writes

$$\begin{array}{rl} \text{piston problem:} & m\ddot{X} + d\dot{X} + kX = c^2 \Delta\rho(L) \\ \text{box problem:} & m\ddot{X} + d\dot{X} + kX = c^2(\Delta\rho(L) - \Delta\rho(0)) \end{array} \tag{10}$$

The reader shoul notice that both linearized problems are set on $[0; L]$. Since W already is a perturbation, the preceding approximation produces an error of the second order in perturbations.

We now have to find the different modes of each linear problem. In the following, we will limit our investigations to the cases where $d = 0$. When $d > 0$, the system is naturally damped. When $d < 0$, the system is naturally undamped and unstable. The importance of the case where $d = 0$ should be emphasized. In that case, the physical system is just stable. Thus, the numerical qualities of the simulation are directly related to numerical properties of the integration methods, particularly in terms of stability.

We first consider the piston problem. A solution of (8) with the "left" boundary condition $\Delta u(0) = 0$ is given by

$$W = \begin{pmatrix} 1 \\ +c \end{pmatrix} \cos[\omega(t - \frac{x}{c})] + \begin{pmatrix} 1 \\ -c \end{pmatrix} \cos[\omega(t + \frac{x}{c})] \quad (\text{with } \omega \in I\!R). \tag{11}$$

If we assume a coupled mode of the preceding form exists, then for this mode we have:

$$\dot{X} = \Delta u(L) = \frac{2c}{\rho_0} \sin(\frac{\omega L}{c}) \sin(\omega t) \quad \text{which gives} \tag{12}$$

$$\ddot{X} = \frac{2c\omega}{\rho_0} \sin(\frac{\omega L}{c}) \cos(\omega t) = -\omega^2 X \tag{13}$$

On the other hand, the density perturbation at the right moving end of the piston is given by

$$\Delta\rho(L) = 2\cos(\frac{\omega L}{c}) \cos(\omega t). \tag{14}$$

Finally, the structural equation (10) for the piston is verified (with $d = 0$) if and only if the following relation is true:

$$\boxed{\text{Piston problem: } \left(\frac{\omega L}{c}\right) \tan\left(\frac{\omega L}{c}\right) \left(1 - \frac{k}{m\omega^2}\right) = \frac{\rho_0 L}{m}.} \tag{15}$$

This formula deserves several comments. We see that when the piston is given an inifinite mass (i.e. is fixed), we find an infinity of purely acoustic modes in the fluid part of the piston problem. We also see that if the piston is given a fixed structural eigenfrequency, and if its mass is big enough compared to ρ_0, the coupled eigenfrequencies get closer to this structural

eigenfrequency. Finally, we can notice that the lowest coupled pulsation is greater than the structural pulsation $\omega_s = \sqrt{k/m}$ (when the latter is smaller than the lowest purely acoustic pulsation). In that case, the structure is not slowed by the fluid. On the contrary, the system undergoes oscillations which are rather acoustic.

We now consider the box problem. A solution of (8) with the boundary condition for the moving box $\Delta u(0) = \Delta u(L)$ is given by

$$W = \begin{pmatrix} 1 \\ +c \end{pmatrix} \cos[\omega(t - \frac{x-L}{c})] - \begin{pmatrix} 1 \\ -c \end{pmatrix} \cos[\omega(t + \frac{x}{c})] \quad (\text{with } \omega \in I\!R). \tag{16}$$

We assume again a coupled mode of the preceding form exists. We then have:

$$\dot{X} = \Delta u(0) = \Delta u(L) = \frac{c}{\rho_0} \left(\cos(\omega t) + \cos[\omega(t + \frac{L}{c})] \right) \quad \text{which gives} \tag{17}$$

$$\ddot{X} = -\frac{\omega c}{\rho_0} \left(\sin(\omega t) + \sin[\omega(t + \frac{L}{c})] \right) = -\omega^2 X \tag{18}$$

On the other hand, the density perturbations at the ends of the box are given by

$$\Delta\rho(0) = \cos[\omega(t + \frac{L}{c})] - \cos(\omega t) = -\Delta\rho(L) \tag{19}$$

Finally, after some short algebric transformations, we find the structural equation (10) for the box problem is verified (with $d = 0$) if and only if the following relation is true:

$$\boxed{\text{Box problem: } \frac{\rho_0 L}{m} \tan\left(\frac{\omega L}{2c}\right) = \left(\frac{\omega L}{2c}\right)\left(\frac{k}{m\omega^2} - 1\right)} \tag{20}$$

We should compare this formula to the preceding one. When the box is given an inifinite mass, we find an infinity of purely acoustic modes (and their pulsation are doubled, because both ends are now moving). As for the piston case, the coupled eigenfrequency gets close to the structural eigenfrequency if the latter is fixed and the mass of the box tends to infinity. Finally, we notice that the lowest coupled pulsation is smaller than the structural pulsation $\omega_s = \sqrt{k/m}$ (when the latter is smaller than the lowest purely acoustic pulsation). Contrary to the piston case, the structure is slowed by the fluid. The system undergoes oscillations which are not close to acoustic oscillations. These oscillations are closer to those met in buffetting or flutter cases.

2.4 Data sets for test cases

In this section, we want to define a set of test cases for both problems. For a test case, the geometry is set with the equilibrium length of the piston/box L; the fluid equilibrium state definition requires the sound speed c and the density ρ_0; the structure is defined by giving the mass m and the stiffness k (and possibly the damping d if it is not taken equal to zero). However, we can derive from a dimensional analysis that, out of these five data, only two induce

independant variations of the aspect of the test case. In the following, we will set $L = 1$m, $\rho_0 = 1.3$kg/m and $c = 330.332$m/s (this value was deduced from the equation $\rho_0 c^2 = \gamma P_0$ with $\gamma = 1.4$ and $P_0 = 1$atm). A variation of these parameters would be considered as a change in unities of time, length and mass. Test cases will be characterized by the two paramaters m and ω_s (derived from k by $m\omega_s^2 = k$).

In the paper, we consider the following test cases:

- **case 1**: $m = 0.8$kg and $\omega_s = 100$rad/s
- **case 2**: $m = 2.1$kg and $\omega_s = 100$rad/s
- **case 3**: $m = 40$kg and $\omega_s = 30$rad/s

Cases 1 and 2 are not far from data found in classical aeroelastic problems for a two-dimensional two-degree of freedom NACA airfoil (see [6, 2]). The structure has a mass of the same order of magnitude as the fluid mass involved in the system. The structural pulsation ω_s is rather small compared to the lowest purely acoustic pulsation (which is given by $\pi L \simeq 1038$rad/s for the piston problem). Case 3 is of a different type: the mass of the structure is very important, and the structural pulsation is rather small. The system is strongly influenced by the structure and rather weakly coupled. We should obtain greater performances of our numerical methods for time integration.

3 Numerical methods

The numerical simulation of an aeroelastic problem is two-fold: it requires at least the simulations of the fluid dynamics and the structural mechanics and the use of numerical methods in both domains. On the one hand, the structure is generally discretized using a classical finite element method. For our problems, the structure is reduced to something close to a single material point, since it has only one degree of freedom (which is the displacement X). This moving structure must be integrated in time. We will present in the following a well-known family of time-integration methods used for the strcuture.

On the other hand, the fluid is enclosed in the moving/flexible box. The fluid domain, which will be discretized, is also moving along with the piston or the box. Then, the numerical simulation requires the use of moving grids (at least at fluid domain boundaries). As a consequence, we will have to produce methods for moving the grid (theses methods are rather straightforward for one-dimensional problems). We also have two consider ALE formulations of Euler equations, i.e. formulations with imbedded non physical spatial coordinates. We will have to use numerical methods for the resolution in time and space of these formulations.

Finally, we present in this section the specific numerical methods used for the coupled integration in time and space of the coupled fluid/structure interaction problem. Actually, the simulation of this coupled aeroelastic problem is not strictly reduced to the integration of structural mechanics and of fluid dynamics in a moving domain. The coupling has to be simulated. We will see it can not be simulated in a totally coupled way, because of the use of implicit schemes, at least for the structure. We will then introduce staggering schemes, and finally subcycling methods when the stability limits on the time step for the fluid and the structure are very different.

3.1 Numerical methods used for the structure

In both the piston and the box problems, which are one-dimensional, the structure can be considered as a single material point. Then, no discretization problem appears. However, a classical **finite element** discretization could be used for more complex structures [1, 7]. Throughout this section, we assume the equation for the structure as presented in (5) holds. In the following, we will present numerical methods that are also convenient when m, d and k are square matrices, m and k being definite positive, and d simply positive.

We present here rapidly a general family of methods for the time-integration of structural dynamics: the **generalized-α method** [8]. We suppose the applied force F is known during the integration of the structure. The generalized-α method depends on four coefficients: β and γ (which keep the same role as in Newmark methods [9, 10]), and α_f and α_m (time-shifting coefficients). Superscripts will be reserved for time step ordinals. For any quantity z, for any given parameter θ ($\theta \in I\!R, 0 < \theta < 1$), and for any time step ordinal n, we use the notation

$$z^{n+\theta} \equiv (1-\theta)z^n + \theta z^{n+1}.$$

The generalized-α method can be described as follows:

- assume at time t_n, $X(t_n) = d^n$, $\dot{X}(t_n) = v^n$ and $\ddot{X}(t_n) = a^n$ are known
- assume d^{n+1} and v^{n+1} are given by the following expressions, depending on the unknown quantity a^{n+1} (through $a^{n+2\beta}$ and $a^{n+\gamma}$):

$$d^{n+1} = d^n + \Delta t v^n + \frac{\Delta t^2}{2} a^{n+2\beta} \tag{21}$$

$$v^{n+1} = v^n + \Delta t a^{n+\gamma} \tag{22}$$

- using the preceding assumptions, find a^{n+1} solution of the structural dynamics equation:

$$m a^{n+1-\alpha_m} + d v^{n+1-\alpha_f} + k x^{n+1-\alpha_f} = F^{n+1-\alpha_f} \tag{23}$$

- using (21-22), compute the next time step computational values d^{n+1} and v^{n+1} and set $X(t_{n+1}) = d^{n+1}$, $\dot{X}(t_{n+1}) = v^{n+1}$ and $\ddot{X}(t_{n+1}) = a^{n+1}$

The family of generalized-α methods contains the Newmark methods (with $\alpha_m = \alpha_f = 0$), the HHT-α methods ($\alpha_m = 0$) [11] and the WBZ-α methods ($\alpha_f = 0$) [12]. The accuracy, the stability, the high-frequency and low-frequency dissipations of the method depends on the parameters β, γ, α_m and α_f.

It can be shown [8] that the method is second-order accurate when $\gamma = 1/2 + \alpha_f - \alpha_m$. The method is unconditionnaly stable, provided $\alpha_m \leq \alpha_f \leq 1/2$ and $2\beta \geq 1/2 + \alpha_f - \alpha_m$. Finally, Chung and Hulbert describe an optimal choice of parameters for this method, which is unconditionnally stable, second-order accurate, and has an optimal combination of high-frequency and low-frequency dissipations. In function of the user-specified spectral radius in the high-frequency limit ρ_∞, the method is written:

$$\alpha_m = \frac{2\rho_\infty - 1}{\rho_\infty + 1},\ \alpha_f = \frac{\rho_\infty}{\rho_\infty + 1},\ \gamma = 1/2 + \alpha_f - \alpha_m,\ \beta = \frac{1}{4}(1 + \alpha_f - \alpha_m)^2 \tag{24}$$

In this paper, we will use this method with different values of $\rho_\infty \in [0,1]$. We will also use the classical trapezoidal rule defined by $\gamma = 1/2$, $\beta = 1/4$ and $\alpha_m = \alpha_f = 0$. We would like to put the emphasis on a particular point for more complex simulations: if you consider a linear structure, and you use only linear schemes, like the trapezoidal rule or the generalized-α method, the time integration of the structure requires the solution of a linear system for each time step. If the structural time step Δt_s remains fixed during the simulation, all matrices involved remain constant and can be inverted once and for all. This advantage should be conserved when the time-integration of the fluid part in the staggered methodology is performed simultaneously.

3.2 Numerical methods used for the fluid

In the preceding section, we presented the structural part of the integration of the aeroelastic interaction. The influence of the fluid on the structure is the aerodynamic external force F. In this section, we deal with the fluid part of the simulation. The influence of the structure on the fluid flow is the result of a two-fold boundary condition. From a physical point of view, the structural boundary of the fluid domain matches exactly the boundary of the structure, and the fluid normal velocity near the fluid/structure interface is equal to the interface normal speed. As a consequence, we will present in this section numerical methods which can be used for the simpler simulation of fluid dynamics in a moving domain.

The fluid domain is no longer considered as fixed. The spatial discretization will also be moving, at least at the boundaries. Some numerical experiments have been made on "transpiration" methods, where the grid is fixed everywhere, the fluid/structure interface included, and where transpiration terms were added to compensate for the violation of the matching condition of both fluid and structure interfaces [5]. These kind of methods are efficient for simple linearized cases, and are of lower interest for non-small displacement. However, they would give good numerical estimates for the coupled linear eigenfrequencies of the physical system.

In this paper, we will consider numerical methods with moving fluid grids. The use of this kind of methods is rather simple and general. They are known as Arbitrary Lagrangian-Eulerian formulations. Although they have a general form [13], they can be applied on Euler equations [1]. The latter take the following integral form:

$$\boxed{\frac{d}{dt}\left[\int_{C_x} W\, dx\right] + \int_{C_x} div_x \bar{F}\, dx = 0.} \tag{25}$$

where x is the spatial physical position of a point, C_x is the geometric cell of integration. The boundaries of this cell are assumed to move with the mesh local speed w (depending on x). W is the vector of conservative variables $(\rho, \rho u, E)^t$ and $\bar{F}$ is the ALE-modified flux vector given by:

$$\bar{F} = \begin{pmatrix} \rho\bar{u} & \\ \rho u\bar{u} & +P \\ E\bar{u} & +Pu \end{pmatrix} \quad \text{and} \quad \bar{u} = u - w. \tag{26}$$

From (25), the deduction of a **finite volume explicite scheme** is straightforward. The

numerical method will be written:

$$A_i^{n+1}W_i^{n+1} - A_i^n W_i^n + \Delta t\left(\bar{\Phi}(W_i^n, W_{i+1}^n) - \bar{\Phi}(W_{i-1}^n, W_i^n)\right) = 0, \tag{27}$$

where C_i^n is the i^{th} cell at time t^n (and $C_i^n = [x_{i-1/2}^n, x_{i+1/2}^n]$), W_i^n is the average of W on cell C_i^n at time t_n, A_i^n is the area of cell C_i^n at time t_n, Δt is the time step, and $\bar{\Phi}$ is a numerical flux such that

$$\Delta t\bar{\Phi}(W_i^n, W_{i+1}^n) \simeq \int_{t^n}^{t^n+\Delta t} \bar{F}(x_{i+1/2}^n)d\tau \tag{28}$$

The evolution of A_i^n with the time is given by:

$$A_i^{n+1} - A_i^n + \Delta t\left(-w_{i+1/2}^n + w_{i-1/2}^n\right) = 0, \tag{29}$$

Since the grid points are updated according to

$$x_{i+1/2}^{n+1} = x_{i+1/2}^n + \Delta t w_{i+1/2}^n, \tag{30}$$

(29) is equivalent to

$$A_i^n = x_{i+1/2}^n - x_{i-1/2}^n, \forall i, \forall n \tag{31}$$

The complete method will not be fully described till we give our choice for the numerical flux $\bar{\Phi}$ in (27). Throughout this paper, the time integral of (28) is approximated using the **flux-vector splitting of Van Leer** [14]. The approximation is only taken as **first order** accurate for several reasons: it is quite simpler (though spatial second order accuracy can be achieved with Van Leer fluxes [15] or with the flux-difference splitting of Roe in dynamic meshes [16]), and it allows the use of much lighter first-order time-integration schemes without stability problems. We could also argue that the main goal of the present paper is the investigation of the coupling simulation, which still is complex, even when it is done with simple uncoupled methods.

This splitting takes the following form on dynamic meshes [15, 17]:

$$\bar{\Phi}(W_i^n, W_{i+1}^n) = \bar{\Phi}^+(W_i^n) + \bar{\Phi}^-(W_{i+1}^n) \tag{32}$$

with

$$\bar{\Phi}^{\pm}(W_i^n) = \pm\frac{\rho}{4c}(\bar{u} \pm c)^2.\begin{pmatrix} 1 \\ \frac{\pm 2c - \bar{u}}{\gamma} + u \\ \frac{-(\gamma-1)\bar{u}^2 \pm 2(\gamma-1)\bar{u}c + 2c^2}{\gamma^2-1} + \frac{u^2}{2} - \frac{w(\bar{u}\mp 2c)}{\gamma} \end{pmatrix} \tag{33}$$

where we have taken

$$\left|\begin{array}{rcl} \rho &=& \rho_i^n \\ c^2 &=& \frac{\gamma P_i^n}{\rho_i^n} \end{array}\right| \quad \left|\begin{array}{rcl} u &=& u_i^n \\ w &=& w_{i\pm 1/2}^n \end{array}\right| \quad \left|\begin{array}{rcl} \bar{u} &=& u - w \end{array}\right| \tag{34}$$

The preceding expressions for the extended Van Leer flux-vector splitting are always valid under the condition $|\bar{u}| < c$ (we limit this study to subsonic cases).

We now describe the treatment of boundary conditions (4). For both ends of the chamber, the boundary condition is enforced in the following weak sense: the left end boundary flux is taken equal to $(0, P_1, P_1 w_1)^t$ (we recall 1 in the index of the first left cell in the fluid). As well, the right end boundary flux is taken equal to $(0, P_M, P_M w_M)^t$.

Finally, we must put the emphasis on a peculiar point. We do have a choice on the motion of the mesh. The grid velocity at the fluid/structure interface may be fixed. However, we can choose any mesh motion consistent with this condition. In general, the mesh can be considered as a third field for the fluid/structure interaction simulation. It can be given any artificial mass and damping matrices, and integrated like a structure [18]. For instance, Batina [19] proposed a method for the smooth motion of the fluid mesh around a deforming airfoil, which was based on a spring model. This method was compared to a simple change of frame of reference in the case of a rigid motion of the structure [7] and gives good results efficiently.

Thoughout the whole paper, we chose to move the fluid mesh in order to have a uniform cell size at any time. For the box problem, all points are given the same speed (and cells keep the same contant size). Though the box is rigid in that case, we kept the dynamic mesh formulation. Assuming we have M points in the mesh, the mesh motion is given by

$$\forall i, \quad 1 \leq i \leq M, \quad x_i^n = \frac{i-1}{M-1} L + X^n \quad \text{and} \quad w_i^n = \dot{X}^n. \tag{35}$$

For the piston problem, all grid speeds vary in proportion with the distance from the fixed left end of the chamber:

$$\forall i, \quad 1 \leq i \leq M, \quad x_i^n = \frac{i-1}{M-1} (L + X^n) \quad \text{and} \quad w_i^n = \frac{i-1}{M-1} \dot{X}^n \tag{36}$$

3.3 Coupling numerical methods...

In this section, we deal with numerical methods which are needed for the simulation of coupled fluid and structural fields. We presented in the two previous sections methods for the simulation of structural dynamics and fluid dynamics on a moving domain, which are not coupled systems. The goal of this section is two-fold: introduce methods directly needed by the coupling phenomenon, and couple both sets of uncoupled methods presented earlier.

In this paper, we only consider staggering strategies. They consist in the successive decoupled integrations of the structure and the fluid. Each field is frozen during the time integration of the other field. This kind of strategy has many advantages. First, the use of existing schemes, programs and procedures for both separate fields can be advocated. It allows also to imagine intra-field and inter-field parallel implementation of the schemes [3]. Second, the use of implicit schemes in a totally coupled time integration scheme would induce a terrible computational cost, because the grid position and velocity would be a numerical variable as well. On the other hand, this kind of staggering scheme may not be stable, even if both the schemes used for separate fields are used far under stability limits. However, the investigation of staggering schemes for one-dimensional linear model problems has recently produced some results [3].

The basic line of a first family of staggering algorithms could be sketched as follows:

- assume you dispose of all computational values after the nth time step. They are the structural displacements, speeds and possibly accelerations on all discretization points (or elements), but also the location and speed of all fluid grid points, and, of course, the field of conservative variables vector W in the whole fluid mesh. We will denote respectively these computational values by S^n (all structural informations), M^n (for the fluid mesh) and W^n for the fluid field.

- compute the distribution of forces and moments exerted by the fluid pressure on the structure (through the fluid/structure interface)
- assume it is constant during the next time step and compute the state of the structure after the next time step (getting S^{n+1}).
- compute a possible fluid grid after the current time-step. The future grid M^{n+1} must satisfy the condition that both fluid and structural boudaries are matching along the interface at time t^{n+1}.
- compute the average speed of each fluid grid point during the current time step.
- use this speed field for the time-integration of the fluid, and get F^{n+1}.

This methodology is the most popular. All steps seem clear and natural. It is "volume-continuous" in the following sense: even though the fluid and the structure may be discretized in different ways, both continuous boundaries (boundaries before discretization) are spatially matching; near the interface, the whole volume is occupied either by the fluid or by the structure. This kind of methods will be refered to as volume-continuous methods.

For these methods, all steps seem clear and natural. However, we will see in the next section that important momentum and energy violations are induced, limiting the stability of the global algorithm. The preceding algorithm can be understood as "integrate the structure and then the fluid, and do it again..." But the symmetrical algorithm "integrate the fluid and then the structure, and so on..." is also possible (the reader should note that the following second methodology differs from the first one by more than an index change !):

- assume you dispose of all computational values after the nth time step S^n, M^n ans W^n.
- make a prediction for the global state of the structure at time t^{n+1}. This prediction could be made with an actual integration of the structure under a constant pressure equal to P^n. However, it could be done simply with a first-order explicit linear predictor.
- compute a possible mesh M^{n+1}a time t^{n+1}, the interface of which must be matching the location for the fluid/structure interface at time t^{n+1} just predicted.
- compute average speed of all fluid grid points during the current time-step.
- perform the time-integration of the fluid part of the problem with these mesh speeds (getting W^{n+1}).
- compute a good approximation of the time integral of the pressure forces and moments around the structure during the current time-step.
- perform the time-integration of the structure and get S^{n+1}.

The most significative difference between both methodologies is the matching condition on the fluid/structure interface. In the second method, there is no matching requirement for the fluid and the structural boundaries after each time-step. With no consideration of spatial discretizations of the fluid and the structure near their interface, we do not assume that both continuous boundaries are matching any more. We have relaxed the matching hypothesis on the continuous boundaries. This kind of methods will be refered to as volume-discontinuous methods.

This methodology seems to allow strong numerical errors at the interface. However, if the prediction of the next location of the structure is accurate, the matching of the interfaces will be achieved with a possibly satisfying accuracy. On the one hand, the matching condition is relaxed, and satisfied with a limited accuracy. On the other hand, the time-integration of the structure might be done with more accuracy, because the fluid pressure distribution at the end of the current time-step (at time t^{n+1}) is already known. Advantages and drawbacks of these two methodologies will be further discussed in the following section. We should put the emphasis on the fact that the volume conservation for the fluid will be written on the fluid volume only, so that we can keep the conservation properties of our schemes.

Finally, we introduce here the principle of subcycling. The time integration of the structure will be done with the generalized-α method or the classical trapezoidal rule (Newmark method with $\gamma = 1/2$ and $\beta = 1/4$) which are both unconditionnaly stable. However, if the lowest coupled pulsation of the system ω_c can be estimated thanks to (15) and (20), the use of a time-step greater than $1/\omega_c$ will produce very inaccurate results. The limit $\Delta t_S^{lim} = 1/\omega_c$ corresponds to six points per oscillations, which gives a rather poor representation of a sinusoidal curve. In the same way, since we will use a simple forward-Euler first-order scheme for the time-integration of the fluid, the time step Δt_f will be limited by a CFL-like condition [7]:

$$\Delta t_f^{lim} = \min_i \frac{\Delta x_i^n}{|\bar{u}_i^n| + c_i^n}, \tag{37}$$

where c_i^n is the local sound speed (equal to $(\gamma P_i^n/\rho_i^n)^{1/2}$). Throughout this paper, the chamber is given in both problems a length unity. And the fluid grid was made of fifty points (and fifty cells around these points). The experience proves that, for industrial cases like those discussed in [6, 2], the limit time step for the structure integration Δt_S^{lim} can be very large compared to Δt_W^{lim}.

This gives the idea of subcycling the fluid. Since the integration of both fields is decoupled in staggering schemes, there is no need to integrate them with the same time step. The only constraint is to advance in time both fields with the same quantity, but not necessarily in the same number of steps. Furthermore, the last step of the first methodology and the fifth step of the second can be performed in a subcycled way: the grid points speeds are only needed. For instance, they could be fixed for each group of subcycles without difficulties. The subcycling can enhance the performance of a code, because it (usually) reduces the number of structural integrations. It also enhances the accuracy of the time-integral of the fluid forces and moments on the structure mentionned in the second methodology. This may be an additional advantage. Last but not least, we already have advocated the use of a constant structural time step Δt_s when we use linear schemes for the linear structures. Since the fluid equations are not linear, and since the stability conditions for the corresponding schemes are not constant throughout the computation (see (37) which is clearly time-dependant), the use of subcycling is necessary: it allows to keep Δt_s constant while Δt_f varies. Another solution would consist of the limitation of the fluid time-step Δt_f uniformly to a smaller value, in order to keep a constant time step and verify (37). This would affect the efficiency of the method as well.

In the following sections, we describe and comment the results given by both methodologies. They must be compared in terms of stability for the limit time-step Δt_S^{lim} and the limit number of subcycles for the fluid. We should also compare their accuracy (especially phase errors and numerical damping). Finally, the possibilities of enhancements will be discussed.

4 The volume-continuous method

In this section, we review in detail investigations on the first method presented above. Considering both fluid and structural interfaces as common and constantly matching (at least, bfore spatial discretization), we mainly study the effects of subscycling and the numerical schemes for grid speeds on the numerical simulations of our model problems.

4.1 Description of the algorithm

The volume-continuous method is the most direct and natural, and the most popular as well. The basic idea is the following. Assuming we want to use a staggering scheme, and considering we need to know the motion of the mesh for the time integration of fluid dynamics, we should advance the structure, compute a new grid and the average grid speed during the time-step and then advance the fluid in time. The subcycling process can be added to the general idea of the method. We now give a precise sketch of the method:

- Compute the pressure P_M^n on the structure at time t^n. There is no actual computation for our two one-dimensional model problems. However, the external force distribution should be computed at this step in more complex computations, like three-dimensional computations with approximate matching grids [20],
- advance the structure using a generalized-α method or a simple trapezoidal rule using a fixed time-step Δt_s for the structure,
- get the displacement of the structure at time t^{n+1} and compute a new fluid grid location (this can be done directly in one dimension according to (35) or (36). However, more complex methods have been reviewed for multi-dimensional cases in [7]),
- fix a motion law for the fluid grid points during the fluid subcycles: for each grid point, the final location must be equal to the location previously computed,
- advance the fluid part of the problem with multiple subcycles, using average grid points speed, depending on the previously defined law of motion. Thoughout this paper, we will denote by N the approximate number of fluid subcycles. N is given by

$$N \simeq \frac{\Delta t_s}{\Delta t_f}. \tag{38}$$

  It is not necessarily an integer. However, we will assume throughout this paper, that N is an integer. In actual numerical simulations, the last subscycle for the fluid is performed with a time step $\widetilde{\Delta t_f}$ that can be smaller than Δt_f, so that we have

$$\Delta t_s = (N-1)\,\Delta t_f + \widetilde{\Delta t_f} \tag{39}$$

  We will also denote by $W^{n,k}$ the fluid state after the k^{th} subcycle. We use the convention that $W^{n,0} = W^n$ and $W^{n,N} = W^{n+1}$.

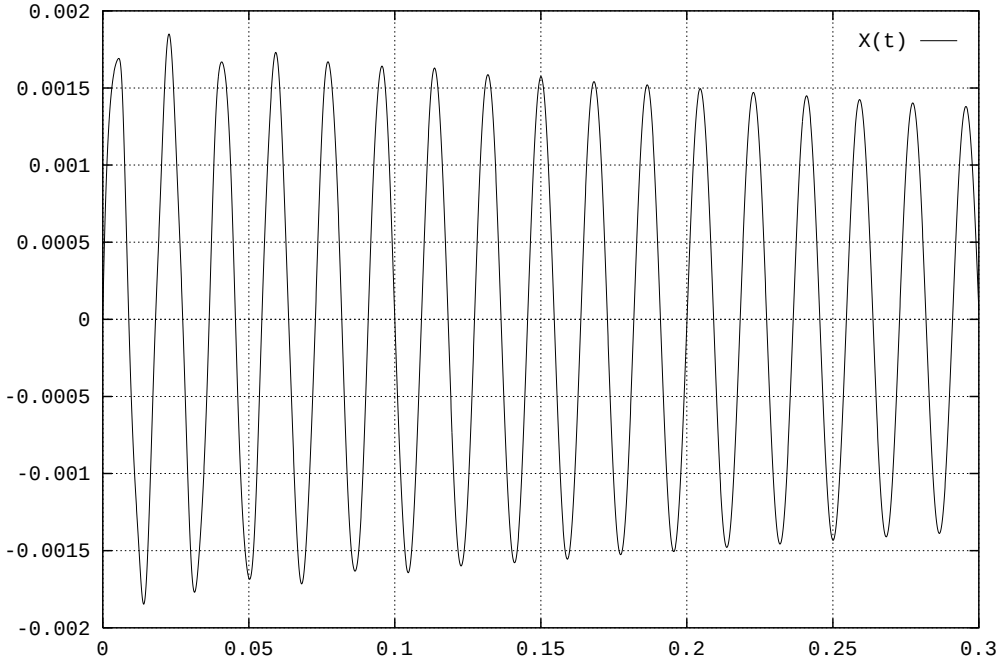

Figure 3: $X(t)$ for the piston problem, **case 1**, $\Delta t_s = 10^{-4}$

4.2 Numerical results

For the first numerical tests, we took for the two last steps the following natural law of motion for the fluid grid points: assuming both displacements x_M^n and x_M^{n+1} are already known, we use:

$$x_M(t) = X_M^n + \frac{X_M^{n+1} - X_M^n}{\Delta t^s}(t - t^n) \quad \text{for} \quad t \in \left[t^n, t^{n+1}\right] \quad (t^{n+1} \equiv t^n + \Delta t_s) \tag{40}$$

which gives a constant average speed for the last grid point w_M during subcycles Δt_f equal to

$$w_M = \frac{X_M^{n+1} - X_M^n}{\Delta t^s}. \tag{41}$$

All remaining fluid grid points locations and speeds were computed according to the simple algorithms (35) or (36). We first applied this algorithm to the piston problem (**case 1**). The structural displacement is presented as a function of time on Figure 3. The structural time step used was $\Delta t_s = 10^{-4}$ which corresponds to an approximate number of subcycles N equal to 4. The result is quite satisfying. The system, which is genuinely physically stable, is added a light numerical viscosity (due to the first order upwind scheme used in the fluid part). However, when we use a bigger time step for the structure, the global scheme becomes unstable. A typical result is showed on Figure 4. The time step $\Delta t_s = 2.6\,10^{-4}$ corresponds to $N = 10$.

This result for the piston problem is not specific. We have made the same numerical tests with the box problem (with **case 2**). We present on Figure 5 (resp. Figure 6) the box displacement in function of time for $\Delta t_s = 2 * 10^{-4}$ (resp. $\Delta t_s = 3 * 10^{-4}$), which corresponds to $N = 8$ (resp. $N = 11$).

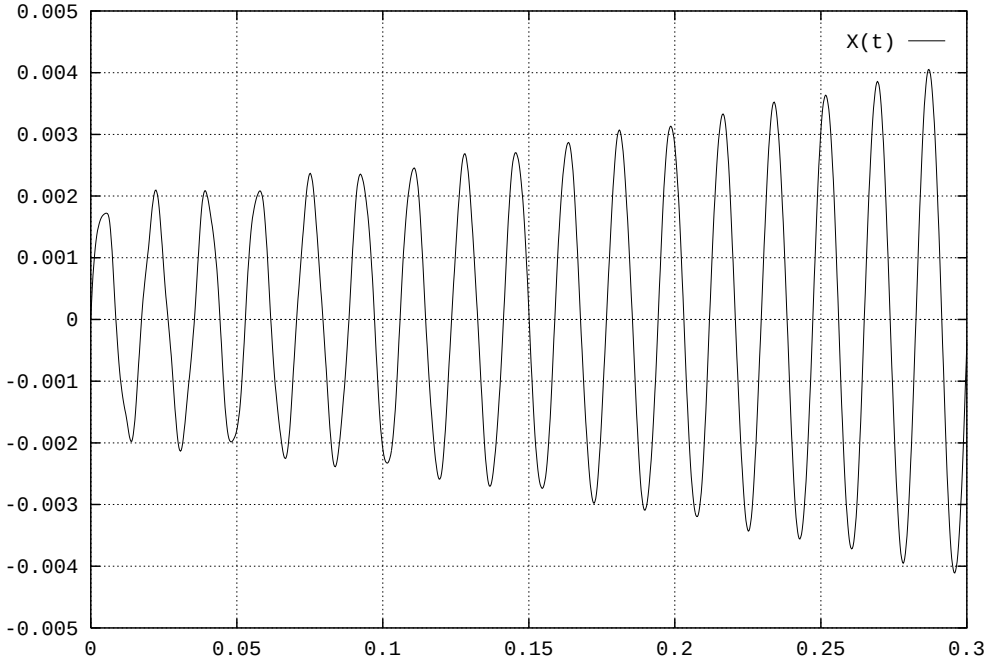

Figure 4: $X(t)$ for the piston problem, **case 1**, $\Delta t_s = 2.6 * 10^{-4}$

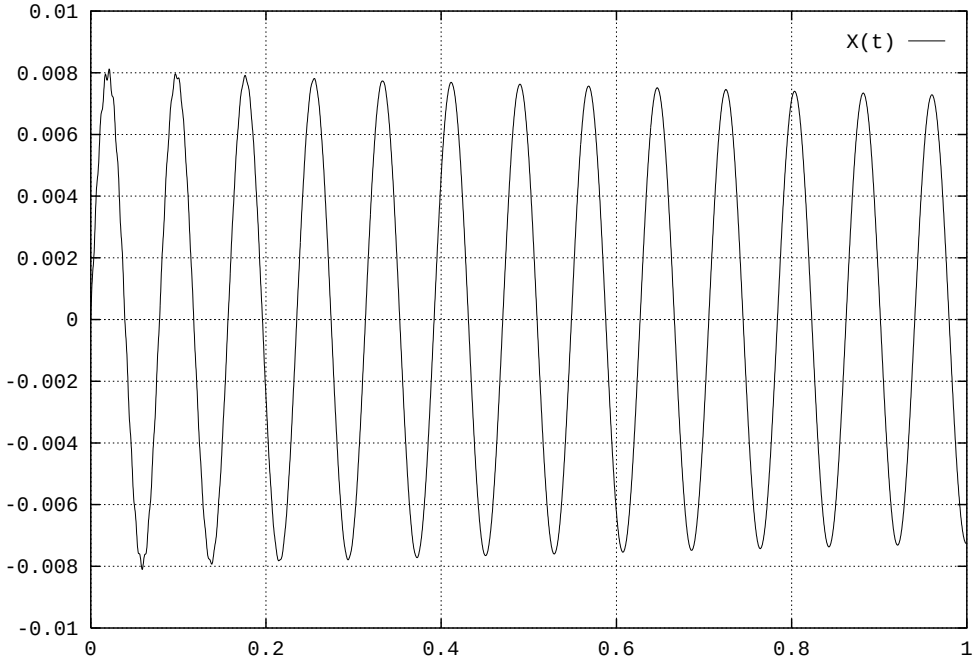

Figure 5: $X(t)$ for the box problem, **case 2**, $\Delta t_s = 2 * 10^{-4}$

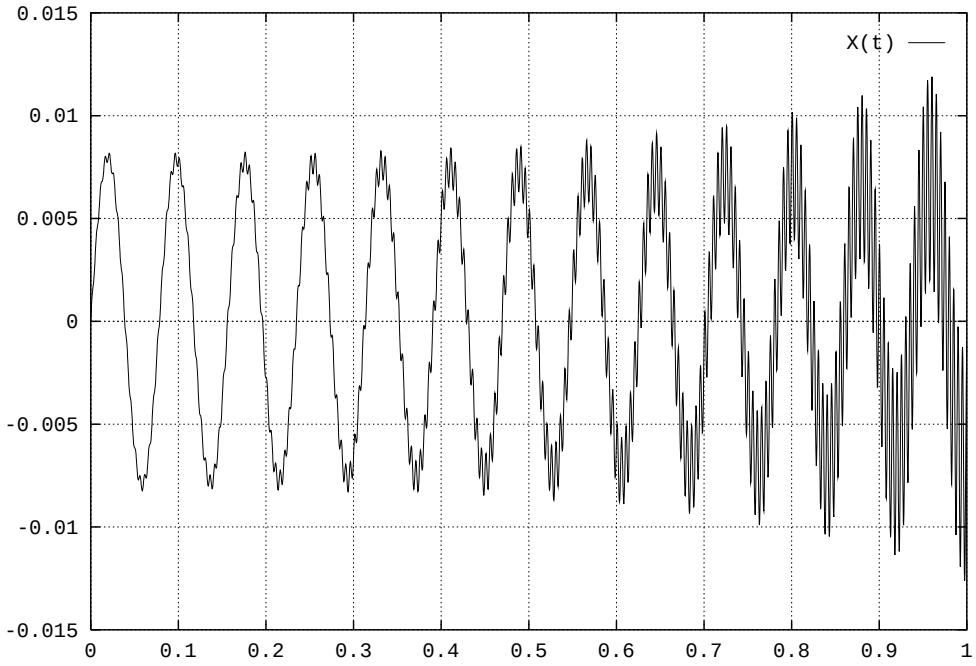

Figure 6: $X(t)$ for the box problem, **case 2**, $\Delta t_s = 3 * 10^{-4}$

They were also described in [3]. We intend to give an simple explanation of the unstability induced by the staggering subcycled algorithm we used. We present on Figure 7 the relative variation of the total energy of the system for the same numerical test as in Figure 6. We can see it increases exponentially. We will show in the following that this algorithm does not conserve the global energy, though we use a conservative scheme for the fluid.

4.3 Discussion on conservation

For instance, let us consider the box problem. We consider the global energy $\mathbf{E}$ of the system. We also denote by $\mathbf{E_f}$ and $\mathbf{E_s}$ respectively the energy of the fluid and the structure. Before spatial discretization, these energies can be written as:

$$\mathbf{E}(t) = \overbrace{\int_{X(t)}^{L+X(t)} E(t,x)dx}^{\mathbf{E_f}(t)} + \overbrace{\frac{1}{2}m\dot{X}(t)^2 + \frac{1}{2}kX(t)^2}^{\mathbf{E_s}(t)} \tag{42}$$

After spatial discretization, we define all corresponding discrete energies by:

$$\mathbf{E}^n = \overbrace{\sum_{i=1}^{M} A_i^n E_i^n}^{\mathbf{E_f}^n} + \overbrace{\frac{1}{2}m\dot{X}^{n^2} + \frac{1}{2}kX^{n^2}}^{\mathbf{E_s}^n} \tag{43}$$

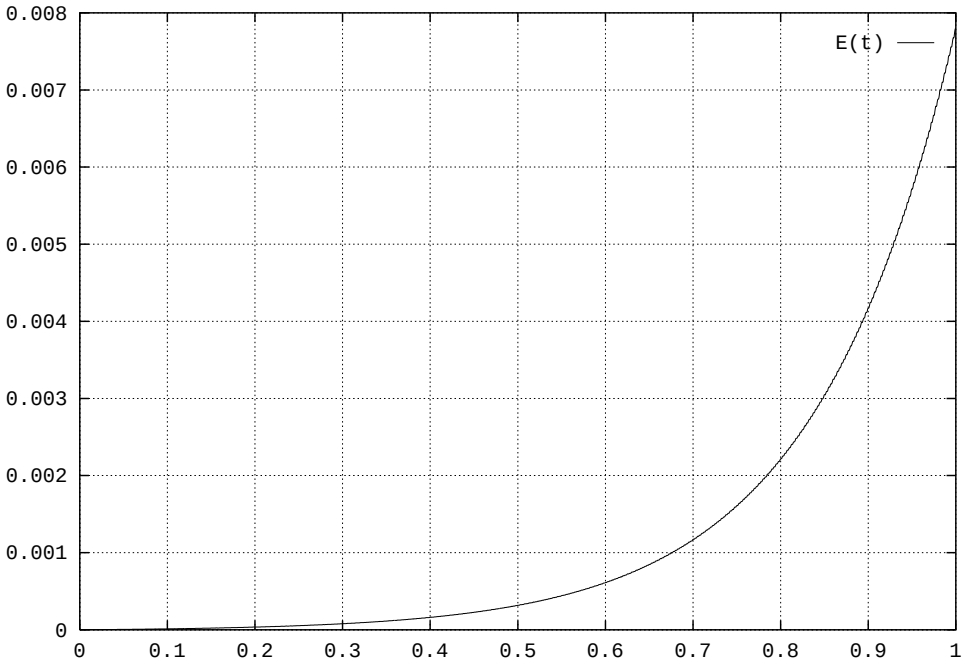

Figure 7: $E(t)$ for the box problem, **case 2**, $\Delta t_s = 3 * 10^{-4}$

We assume we use a trapezoidal rule for the time-integration of the structure. During the time step Δt_s, the fluid exerts a pressure at both ends taken as constant on the structure, and equal to P_1^n and P_M^n. Thus, it is easily showed that the energy variation for the box is given by:

$$\mathbf{E_s}^{n+1} - \mathbf{E_s}^{n} = \Delta t_s \left(P_M^n - P_1^n\right) \frac{\dot{X}^n + \dot{X}^{n+1}}{2}$$

The trapezoidal rule has the property that the preceding equation reduces to

$$\mathbf{E_s}^{n+1} - \mathbf{E_s}^{n} = \left(P_M^n - P_1^n\right) \left(X^{n+1} - X^n\right) \tag{44}$$

On the other hand, the energy variation for the fluid during each subcycle Δt_f depends only on the boundary fluxes given on page 10, because we use the conservative scheme (27). This variation is given by:

$$\mathbf{E_f}^{n,k+1} - \mathbf{E_f}^{n,k} = -\Delta t_f \left(P_M^{n,k} w_M^{n,k} - P_1^{n,k} w_1^{n,k}\right)$$

Since the mesh velocity is constant and equal to $(X^{n+1} - X^n)/\Delta t_s$, we have:

$$\mathbf{E_f}^{n,k+1} - \mathbf{E_f}^{n,k} = -\frac{1}{N} \left(P_M^{n,k} - P_1^{n,k}\right) \left(X^{n+1} - X^n\right). \tag{45}$$

Finally, the total energy variation for the fluid through all subcycles is given by:

$$\mathbf{E_f}^{n+1} - \mathbf{E_f}^{n} = -\frac{1}{N} \left[\sum_{k=0}^{N-1} \left(P_M^{n,k} - P_1^{n,k}\right)\right] \left(X^{n+1} - X^n\right). \tag{46}$$

Since the pressure distribution varies during the fluid subcycles, we have as a consequence:

$$\mathbf{E}^{n+1} - \mathbf{E}^n = \frac{1}{N}\left[\sum_{k=0}^{N-1}\left[\left(P_M^n - P_M^{n,k}\right) - \left(P_1^n - P_1^{n,k}\right)\right]\right]\left(X^{n+1} - X^n\right) \neq 0 \tag{47}$$

The preceding equation should be interpreted the following way. Though the physical system receives no external work (fixed end of the spring, and equal external pressure on both ends of the box, which are moving at the same speed), the total energy is not conserved. It means that the respective works of the force exerted by the fluid on the structure and the force exerted by the structure on the fluid were not computed as opposite. The careful reader should already have noticed that these forces themselves were not computed as opposite but respectively as:

$$Force[\text{Fluid} \rightarrow \text{Box}] \overset{\text{comp. as}}{=\!=} \Delta t_s \left(P_M^n - P_1^n\right) \tag{48}$$

and

$$Force[\text{Box} \rightarrow \text{Fluid}] \overset{\text{comp. as}}{=\!=} -\frac{\Delta t_s}{N}\left[\sum_{k=0}^{N-1}\left(P_M^{n,k} - P_1^{n,k}\right)\right]. \tag{49}$$

The preceding results hold for a general Newmark method, not necessarily equal to the trapezoidal rule, provided it is unconditionnaly stable (which is achieved when $2\beta \geq \gamma \geq 1/2$). The difference is a simple numerical dissipation in the structural part of the integration. This remark holds also for the generalized-α method.

The unstability of the staggered subcycled scheme can be explained the following way. The discrepancy between exchanged works or exchanged forces at the fluid/structure interface increases as the number N of subcycles (and Δt_s) gets bigger. This difference induces variations on the eigenvalues of the transformation matrix (matrix operating on numerical values at time t^n to obtain numerical values at time t^{n+1}). When the time step Δt_s is small enough, these eigenvalues have a modulus less than one (because of numerical viscosity, the scheme is stable at least for a small N). As N increases, the perturbation increases, and a modulus greater than one appears when N increases.

On Figure 4 and Figure 6, we showed two results of unstable simulations where the subcycle factor N was beyond stability (respectively $N = 10$ and $N = 11$). But there is no explicit expression for the stability limit on N (such as "$N < 12$" or whatever). The limit is rather put on the dimensionless numbers $\omega_c \Delta t_s$ or $\omega_s \Delta t_s$ which have to be small compared to unity (we write $\omega_s \equiv \sqrt{k/m}$ for the eigenpulsation of the structure and we recall ω_c is the lowest coupled eigenpulsation of the physical system). For example, we show on Figure 8 a simulation of the box problem with **case 3** where we obtain a stable simulation with $\Delta t_s = 3 * 10^{-3}$ which corresponds to $N = 109$. Though N is huge, we have $\omega_c \Delta t_s = 0.09 \ll 1$.

We show on Table 1 the set of stability limits we found for both problems in the first two cases. We can notice the order of magnitude of the non-dimensionalized time step $\omega_c \Delta t_s$ where the method becomes unstable is near 1% which corresponds to six hundred points per period of oscillation (which is a lot too much!). This also holds for **case 3** where a lot of points per coupled period of oscillation was needed. We were not able to produce the lines corresponding to the last case in the preceding table, because the structural mass is so important that the energy production described earlier (inducing unstability) has a visible effect after a huge number of time-step. However, we know the method is certainly less stable that it seems to be.

As a conclusion, we emphasize the fact that the volume-continuous method, has a very low stability limit, since for most cases, it requires the use of several hundreds of elementary time-integrations for each period of coupled oscillation. This method is currently used in all industrial

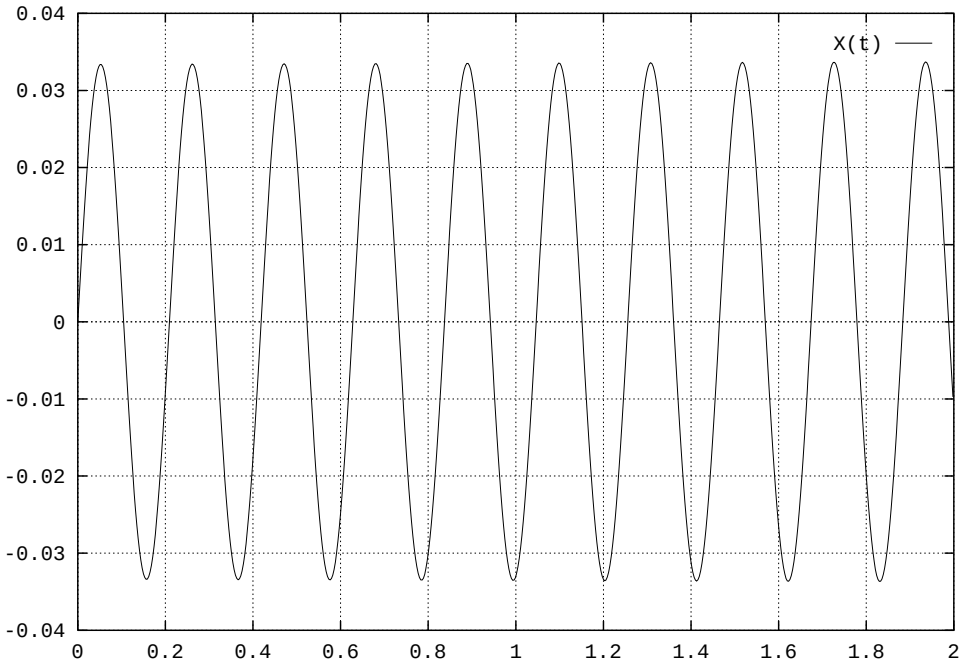

Figure 8: $X(t)$ for the box problem, **case 3**, $\Delta t_s = 3 * 10^{-3}$

Table 1: Stability limits on Δt_s for both problems in **cases 1 and 2**.

problem	test case	$\omega_s\ (rad/s)$	$\omega_c\ (rad/s)$	$\Delta t_s\ (s)$	N	$\omega_s \Delta t_s$	$\omega_c \Delta t_s$
piston	**case 1**	100	344	$1.5 * 10^{-4}$	6	$1.5 * 10^{-2}$	$5.20 * 10^{-2}$
piston	**case 2**	100	253	$1.3 * 10^{-4}$	5	$1.3 * 10^{-2}$	$3.29 * 10^{-2}$
box	**case 1**	100	61.7	$1.5 * 10^{-4}$	6	$1.5 * 10^{-2}$	$0.93 * 10^{-2}$
box	**case 2**	100	78.5	$2.6 * 10^{-4}$	10	$2.6 * 10^{-2}$	$2.04 * 10^{-2}$

aeroelastic computations. We intend to present in the next section a new method where the matching condition on interfaces is relaxed. We will show that this method is not perfect (it is not unconditionnaly stable), but has reduced drawbacks compared to the method presented in this section. At this point, the reader should remember that the volume-conitunuous method produces a violation of the principle of action and reaction (for the contact forces at the fluid/structure interface) in terms of momentum and energy. In the following section, we present a new method with relaxation of the matching condition for interfaces. We show that this method preserves in a more satisfying way the momentum and energy conservation through the fluid/structure interaction.

5 Volume-discontinuous method

In this section, we present a new method for the numerical simulation of a one-dimensional aeroelastic model problem. We show the enhancement proposed and discuss numerical results of the method. We also present some complementary tests based on classical ideas, like predictor-corrector loops and numerical auto-adaptive filters.

5.1 Description of the algorithm

The basic idea of this method is the relaxation of the matching condition on the fluid/structure interface. This idea might seem surprising, since all coupling phenomena take place at this point. However, we intend to relax the matching condition up to a limited point. We will assume and investigate that the non-matching fluid and structural interfaces remain close during the numerical simulation. We will see that this method allows us to get rid of the discomfort of staggering schemes, where the integration in time of a first field is done using a very unaccurate information coming from the other field.

The principle of the method is simple. We assume we do not require that both intefaces match exactly (with no consideration of spatial discretizations of both boundaries), but that they remain close throughout the computation. For each structural time-step (that can be also subcycled for the fluid part), we make a prediction of the state of the structure at the end of the time step. We imagine a fluid mesh motion during the current time step which matches the prediction at the end of the time step. Then we advance the fluid (possibly in a subcycled way). We store the fluid pressure forces on the structure during this integration, and use this pressure distribution for the structural part of the integration. The method is now described with more accuracy:

- compute a prediction of the state of the structure at the end of the current time step Δt_s. This prediction can be more or less complex. The more accurate this prediction is, the more accurate the coupling should be. This prediction will be discussed in this section.
- from the predicted displacement of the structure at time t^{n+1}, compute a new fluid grid location (again, this can be done in a very simple way in one-dimensional problems according to (35) or (36)).

- fix a motion law for the fluid grid points during the fluid subcycles: for each grid point, the final location must be equal to the location previously computed (which matches the location of the structure at the end of the current time step we first predicted).

- advance the fluid part of the problem with multiple subcycles, using average grid points speed, depending on the previously defined law of motion. We will again denote by $W^{n,k}$ the fluid state after the k^{th} subcycle (we recall $W^{n,0} = W^n$ and $W^{n,N} = W^{n+1}$). During each of these fluid time steps, some numerical boundary fluxes are used: $(0, P_1^{n,k}, P_1^{n,k} w_1^n)^t$ and $(0, P_M^{n,k}, P_M^{n,k} w_M^n)^t$ for both problems.

  In the previous expressions, the terms w_1^n and w_M^n do not depend of the integer k, the corresponding index of the subcycle when the mesh speeds have been assumed constant during the subcycles. However, it would not be the case for any different law of motion for the fluid grid points. Anyway, the momentum terms $P_1^{n,k}$ and $P_M^{n,k}$ appear in the momentum equations (5) and (6). For the piston problem, these terms can be seen as the actual force exerted on the fluid and the first term is the force exerted by the fluid on the support of the left fixed end of the chamber. For the box problem, both terms can be interpreted as the forces exerted on the fluid.

  Thus, we can compute the sum of all these momentum terms during the N subcycles (for simplicity reasons, we assume here that $\Delta t_s / \Delta t_f$ is an integer; all following equations could be rewritten with a non-integer fraction $\Delta t_s / \Delta t_f$ as in (39)). The force exerted on the fluid by the box per unit time writes

$$Force[\text{Box} \rightarrow \text{Fluid}] \overset{\text{comp. as}}{=\!=} -\frac{1}{N} \left[\sum_{k=0}^{N-1} \left(P_M^{n,k} - P_1^{n,k} \right) \right] \tag{50}$$

  which is simply deduced from (49), and the force exerted on the fluid by the piston per unit time writes

$$Force[\text{Piston} \rightarrow \text{Fluid}] \overset{\text{comp. as}}{=\!=} -\frac{1}{N} \left[\sum_{k=0}^{N-1} P_M^{n,k} \right] \tag{51}$$

- advance the structure using a generalized-α method or a simple trapezoidal rule using the fixed time-step Δt_s and an external force, which is the opposite of the force we just computed. The great advantage of this method appears clearly. We have enforced the "action and reaction" condition

$$Force[\text{Structure} \rightarrow \text{Fluid}] + Force[\text{Fluid} \rightarrow \text{Structure}] \overset{\text{comp. as}}{=\!=} 0. \tag{52}$$

5.2 Conservation enhancements

We would like to add a few remarks concerning this volume-discontinuous method. We first notice that the method depends of the prediction used in the first step of the algorithm. We have a wide choice for this prediction. Since smaller characteritic times correspond to the structure, the prediction will be rather easy. The error in the predictor will certainly be less important than the error on the external pressure in the first method. We understand also

that the accuracy, or the possible stabilization properties of this prediction enhance the global accuracy and stability of the method.

Second, we have noticed that the global momentum is conserved concerning the interaction (52). We now investigate the conservation of the global energy. Considering the box problem with constant grid points speeds during the subcycles, and using notations defined in (42) and (43), we have again for each subcycle

$$\mathbf{E_f}^{n,k+1} - \mathbf{E_f}^{n,k} = -\Delta t_f \left(P_M^{n,k} w_M^{n,k} - P_1^{n,k} w_1^{n,k} \right).$$

Since the mesh velocity is constant and equal to $(\widetilde{X^{n+1}} - \widetilde{X^n})/\Delta t_s$, we have:

$$\mathbf{E_f}^{n,k+1} - \mathbf{E_f}^{n,k} = -\frac{1}{N} \left(P_M^{n,k} - P_1^{n,k} \right) \left(\widetilde{X^{n+1}} - \widetilde{X^n} \right). \tag{53}$$

where $\widetilde{X^n}$ is the predicted position of the structure after the n^{th} time step. Finally, the fluid energy variation through all subcycles is given by:

$$\mathbf{E_f}^{n+1} - \mathbf{E_f}^{n} = -\frac{1}{N} \left[\sum_{k=0}^{N-1} \left(P_M^{n,k} - P_1^{n,k} \right) \right] \left(\widetilde{X^{n+1}} - \widetilde{X^n} \right). \tag{54}$$

On the other hand, assuming we use a simple trapezoidal rule for the structure, with an external force satisfying (52), the energy variation through one time step writes

$$\mathbf{E_s}^{n+1} - \mathbf{E_s}^{n} = \frac{1}{N} \left[\sum_{k=0}^{N-1} \left(P_M^{n,k} - P_1^{n,k} \right) \right] \left(X^{n+1} - X^n \right). \tag{55}$$

If we write ϵ^n for the mismatching error at time t^n ($\epsilon^n = X^n - \widetilde{X^n}$), the system total energy variation through one time step of this method is given by

$$\mathbf{E}^{n+1} - \mathbf{E}^{n} = \frac{1}{N} \left[\sum_{k=0}^{N-1} \left(P_M^{n,k} - P_1^{n,k} \right) \right] \left(\epsilon^{n+1} - \epsilon^n \right). \tag{56}$$

If the matching error remains small, then the global energy of the system will be conserved with a good accuracy. The preceding equation should be compared to (47). In the preceding equation, the order of magnitude of the energy error depends on the quality of the prediction. Then the error can be reduced not only with a time step reduction (which is not the aim of this paper), but with enhancement of the order of accuracy of the prediction for example. This characteristic induces the great flexibility of the method. On the contrary, (47) proves that the energy conservation error could only be reduced with the use of a prediction of the time-averaged fluid pressure force, which is certainly very difficult to perform (it would require an investigation of the fluid state throughout a thick band of finite volumes cells along the fluid/structure interface). However, the momentum conservation is exactly performed with the second method, and can only be approximately done with the first method coupled with any prediction.

As a second remark, we emphasize here that both interfaces are not matching either at the beginning or at the end of a time step. For our one-dimensional model problems, this characteristic does not make the algorithm more complex. However, the resolution would not be so simple for two- or three-dimensional problems. As a matter of act, fluid pressure forces

on a given fluid interface point should be transmitted to some "corresponding" point of the structural interface. The correspondance could simply be point-to-point, but more complex geometrical methods should be tested.

5.3 Numerical tests

We begin with numerical tests where we have given a constant fluid grid points speed thoughout the subcycles. The mesh locations are given by (40). We note Y^n the position of the right end mesh point after the n^{th} time step ($Y^n = \widetilde{X^n} \neq X^n$). As stated earlier, the volume-discontinuous method is flexible, since several types of predictions can be used. We review in the following some methods of prediction, which could not have been simply coupled with the volume-continuous method.

5.3.1 Explicit first-order prediction (constant speed)

We first try to use the most simple and natural prediction for the structure, which writes

$$\widetilde{X^{n+1}} = X^n + \Delta t_s \dot{X}^n \tag{57}$$

This prediction is only first order accurate, but has the advantage of the simplicity (it can be applied to complex multi-dimensional structures with no computational costs). For each numerical test, we may present two curves, which are the structural displacement X and the mesh displacement (its right end) Y in function of the time. These curves will be compared to those of the preceding section.

We present on Figure 9 these curves for the piston problem in **case 1**. The structural response is correct (same as in Figure 3) at the beginning, but is quite overdamped. The time step used was $\Delta t_s = 0.9 * 10^{-3}$ which is far beyond the time step used in Figure 4 or Figure 5. Figure 10 shows that the scheme is conditionnally stable, and that $\Delta t_s = 1.15 * 10^{-3}$ is beyond the stability limit (which was found to be close to $\Delta t_s = 1.1 * 10^{-3}$). The volume-discontinuous method made possible the use of a time-step (and a subcycling factor N) seven times bigger.

On Figure 11 and Figure 12 are presented the structural displacements in function of time for two numerical simulations of the box problem (**case 2**). When $\Delta t_s = 0.8 * 10^{-3}$, the scheme is stable and gives a result close to Figure 5. In that case, the signal is not overdamped. For $\Delta t_s = 0.86 * 10^{-3}$, the scheme has reached unstability. Spurious mesh oscillations appear. If we look at Figure 13, where the relative variation of the total energy of the system is presented in function of time, we see the global energy relative error increases exponentially like in Figure 7 for the volume-continuous method. However, the stability limit for this case is $\Delta t_s = 0.83 * 10^{-3}$, which is three times bigger than for the first method.

Comparing with the volume-continuous method, we see that this method has an enhanced stability, even when the first one had good results. We present on Figure 14 the structural displacement for the box problem in **case 3**. We see the scheme is stable for a bigger time step ($\Delta t_s = 1. * 10^{-2}$ which corresponds to a subcycling factor $N = 357$ and $\omega_c \Delta t_s = 0.01$!).

Finally, we present in Table 2 the stability limits we found for both problems in **cases 1** and **2** for the volume-discontinuous method. If we compare this table with Table 1, we see a general enhancement for the structural time step Δt_s (and the subcycling factor). The relaxation of

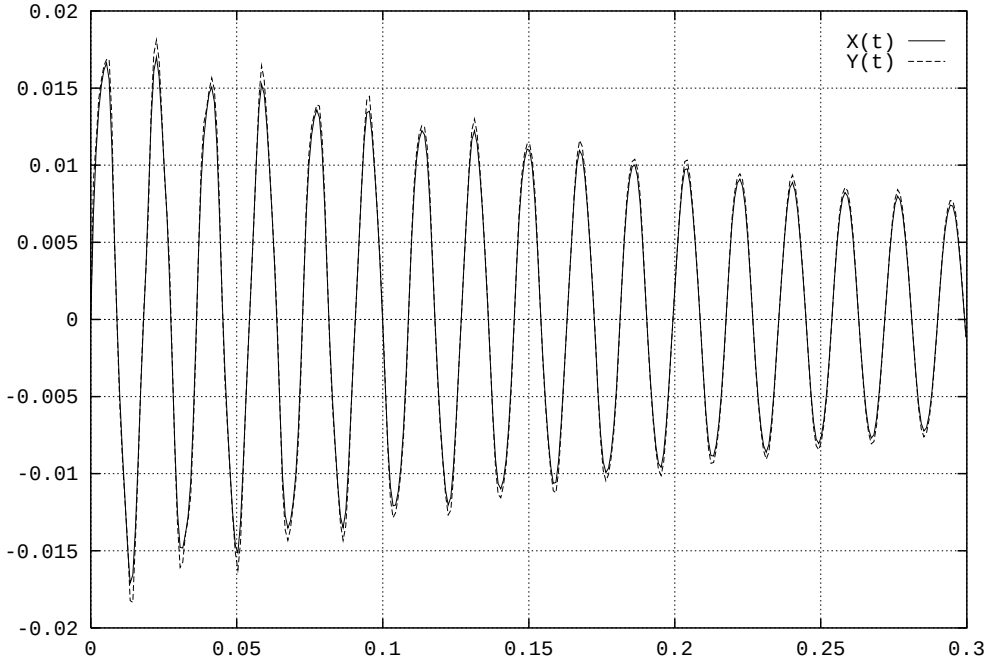

Figure 9: $X(t)$ and $Y(t)$ for the piston problem, **case 1**, $\Delta t_s = 0.9 * 10^{-3}$

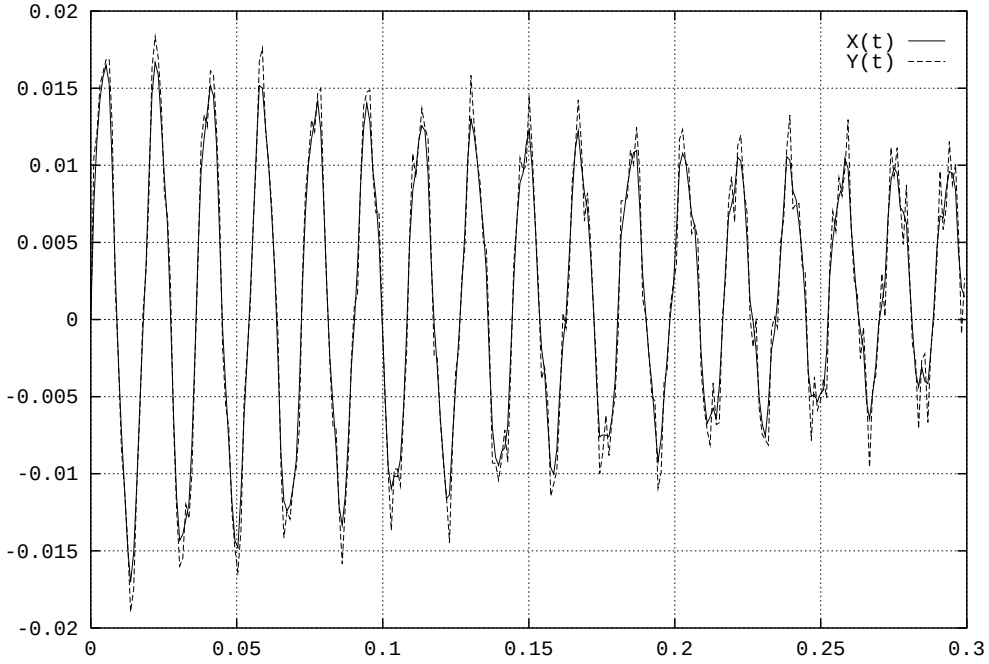

Figure 10: $X(t)$ and $Y(t)$ for the piston problem, **case 1**, $\Delta t_s = 1.15 * 10^{-3}$

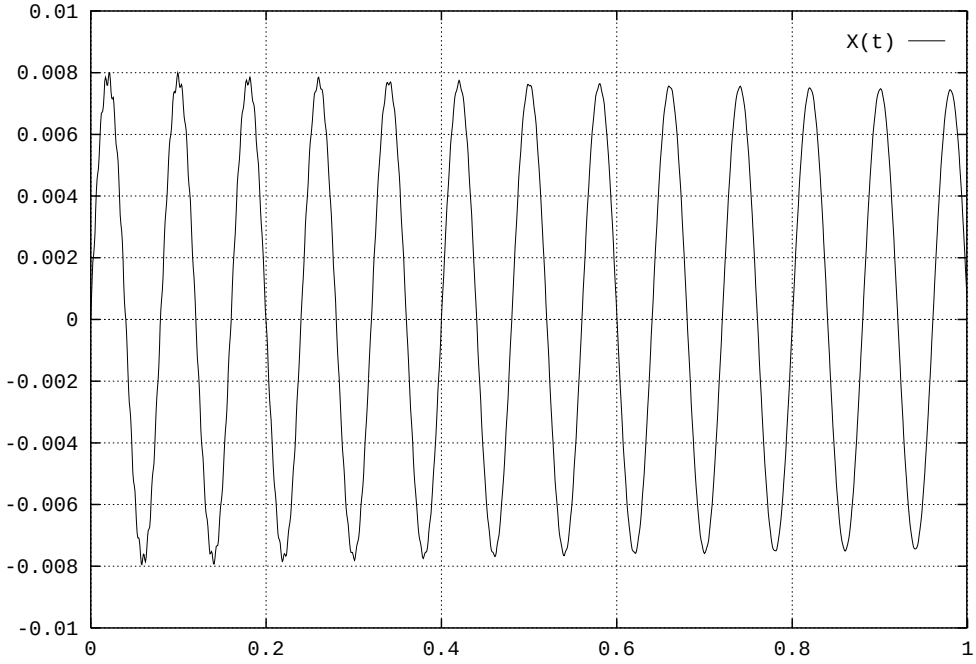

Figure 11: $X(t)$ for the box problem, **case 2**, $\Delta t_s = 0.8 * 10^{-3}$

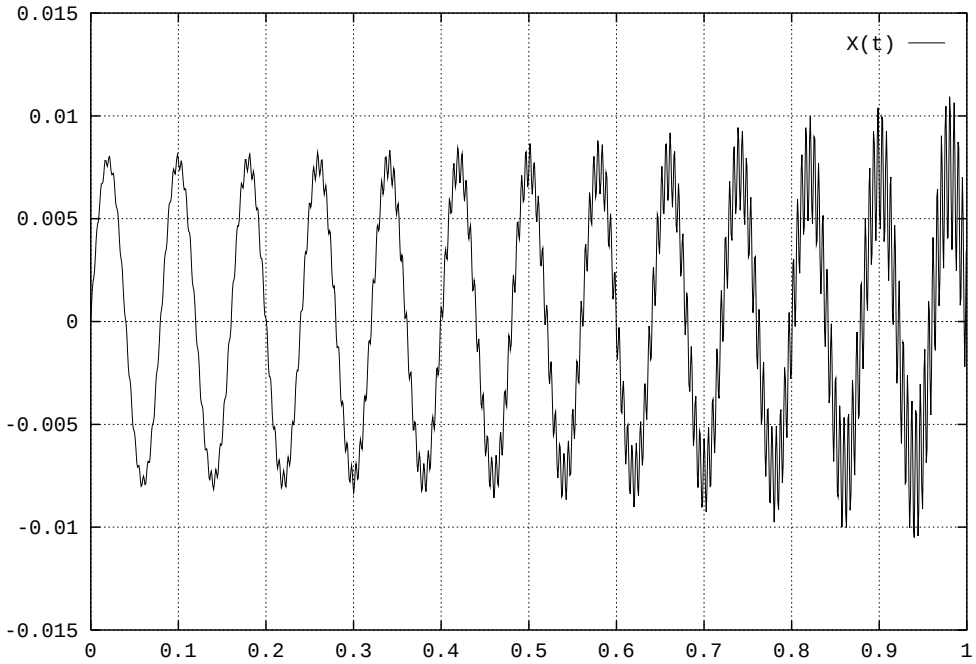

Figure 12: $X(t)$ for the box problem, **case 2**, $\Delta t_s = 0.86 * 10^{-3}$

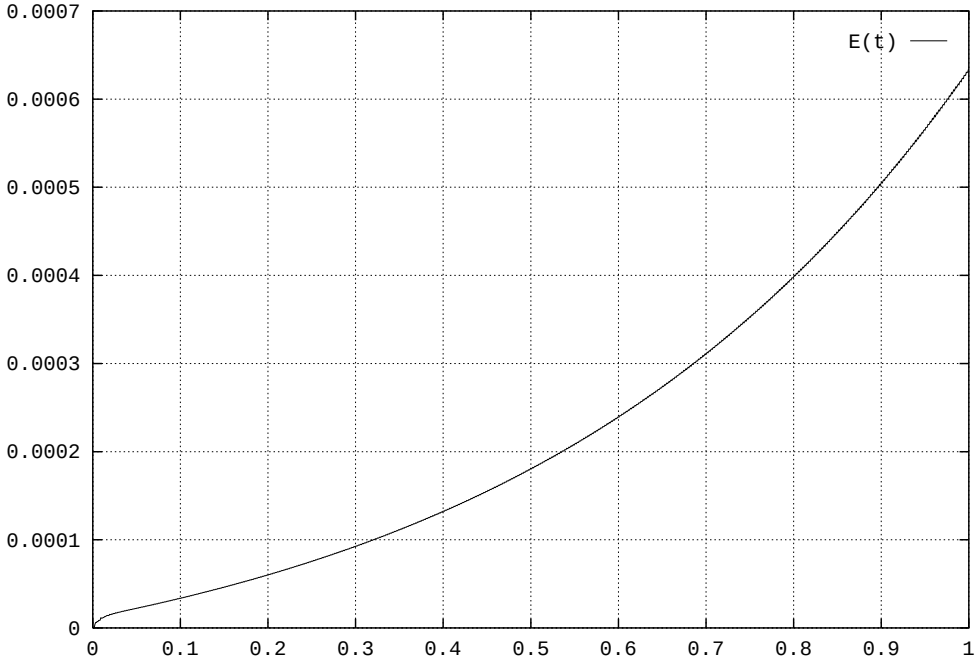

Figure 13: $E(t)$ for the box problem, **case 2**, $\Delta t_s = 0.86 * 10^{-3}$

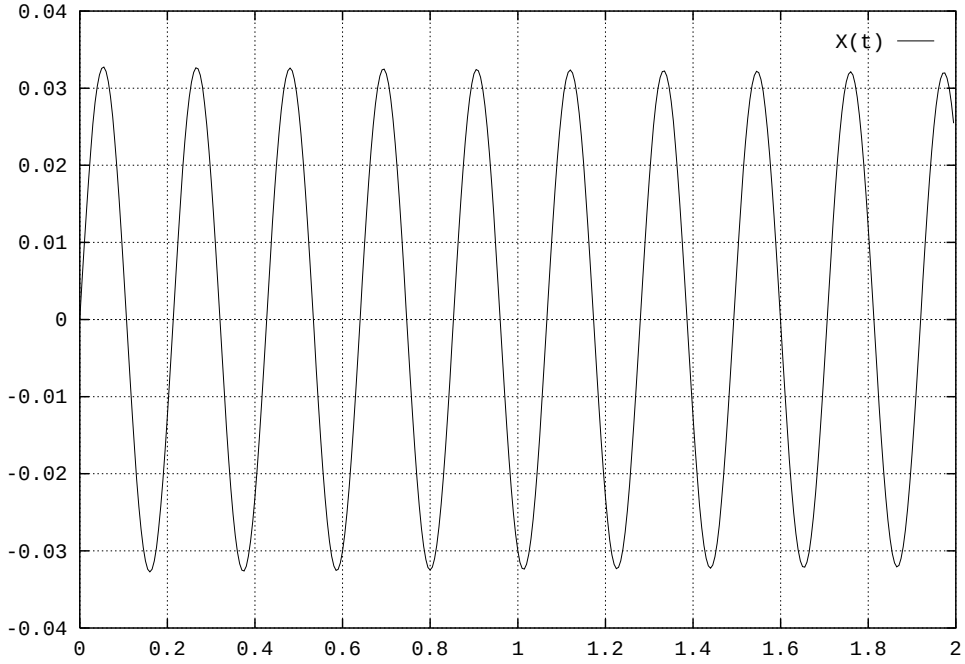

Figure 14: $X(t)$ for the box problem, **case 3**, $\Delta t_s = 1. * 10^{-2}$

Table 2: Stability limits on Δt_s for both problems in **cases 1 and 2**.

problem	test case	$\omega_s\ (rad/s)$	$\omega_c\ (rad/s)$	$\Delta t_s\ (s)$	N	$\omega_s \Delta t_s$	$\omega_c \Delta t_s$
piston	**case 1**	100	344	$1.1 * 10^{-3}$	39	$1.1 * 10^{-1}$	$3.78 * 10^{-1}$
piston	**case 2**	100	253	$1.3 * 10^{-3}$	52	$1.3 * 10^{-1}$	$3.29 * 10^{-1}$
box	**case 1**	100	61.7	$7.0 * 10^{-4}$	26	$7.0 * 10^{-2}$	$4.32 * 10^{-2}$
box	**case 2**	100	78.5	$8.3 * 10^{-4}$	32	$8.3 * 10^{-2}$	$6.52 * 10^{-2}$

the matching condition allowed a better conservation of the energy through the interaction, and an exact conservation for the momentum. The consequence is the gain in stability, though we used the elementary prediction (57).

5.3.2 Explicit second-order prediction (constant acceleration)

In this section, we present a family of prediction method depending of the real parameter θ defined by

$$\widetilde{X^{n+1}} = X^n + \Delta t_s \left[(1+\theta)\dot{X}^n - \theta \dot{X}^{n-1} \right] \tag{58}$$

This prediction is at least first order accurate, and second-order accurate when $\theta = 1/2$. We show on Figure 15 the displacement for the box problem in **case 2**. It is similar to the result given on Figure 11. However, this new method is less stable: the new stability limit is close to $\Delta t_s = 0.78 * 10^{-3}$. We have clearly observed that the enhancement of the accuracy in the prediction method (when it is done in an uncoupled way, independant of the fluid flow) reduces the stability domain of the method. This remark was also valid for other predictions of the following type:

$$\widetilde{X^{n+1}} = X^n + \Delta t_s \dot{X}^n + \theta' \Delta t_S^2 \ddot{X}^n \tag{59}$$

The limited stability of these kinds of predictions is a consequence of their uncoupled nature. For example, the method (58) means the average acceleration during the previous time step has the same value in the current time step. This is equivalent in a certain sense to an assumption on the fluid pressure during the current time step. This aspect could possibly be eliminated with coupled predictions. They will be investigated in the following.

5.3.3 Prediction iterations

We can obtain a coupled method of prediction by iterating the procedure described in 5.3.1. We propose the following algorithm:

-0- at time t^n (i.e. after the n^{th} time step) store the fluid state, the fluid grid and the structural state. set $ipc = 0$

-1- compute a prediction of the structural displacement at time t^{n+1} according to (57)

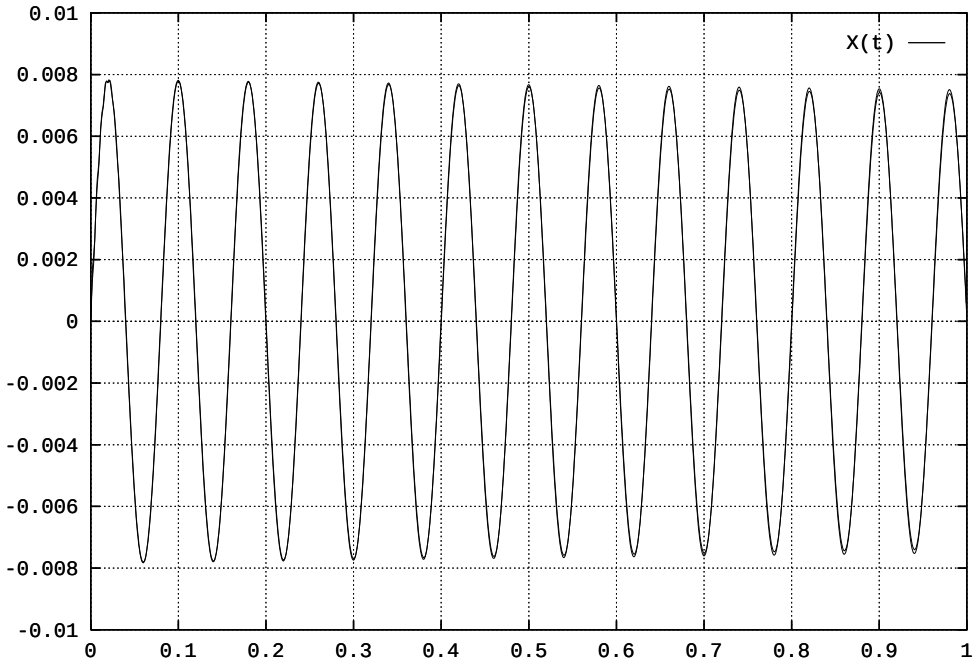

Figure 15: $X(t)$ for the box problem, **case 2**, $\Delta t_s = 0.75 * 10^{-3}$

-2- using this prediction for the structure, compute a fluid mesh at time t^{n+1} and average mesh speeds for the current time step. Using subcycles, advance the fluid in time and store the time-averaged fluid pressure on the structure according to (50-51).

-3- advance the structure till t^{n+1} with the preceding external pressure.

-4- If $ipc < IPC$, use the structural displacement at time t^{n+1} as a prediction, reset all computational values to the values stored at step **0**. $ipc = ipc + 1$ and go to step **2**.

We notice that for each time step, the computational cost is IPC times bigger, since IPC steps of the regular volume-discontinuous method are done. The storage for this method is also double, since we have to store all computational values before each prediction cycle. We show on Figure 16 the performance of this method for the piston problem in **case 1**. We used $IPC = 2$, with $\Delta t_s = 1.8 * 10^{-3}$, which is the double of the time step used in Figure 9. Then computational costs are comparable for the structural part. For the fluid part of the problem, the time step is fixed by a CFL-like condition and in all cases, the computational cost is IPC times bigger. The method is stable. We have increased its stability domain. We emphasize the fact that the preceding time step corresponds to $\omega_c \Delta t_s = 0.756$ which is a rather poor resolution for each coupled period. This explains why the solution is so much damped. The same test for $IPC = 4$ and $\Delta t_s = 3.6 * 10^{-3}$, (which gives $\omega_c \Delta t_s = 1.51$ and means we have only four points per period) which induces again a comparable computational cost for the structure, produced an even more damped solution.

For the box problem (in **case 2**), the result is more interesting. The present iterated method with $IPC = 2$ does not show unstability for $\Delta t_s = 3.2 * 10^{-3}$ (a time step four times bigger than the time step used for the test of Table 2). The displacement for this test is shown on

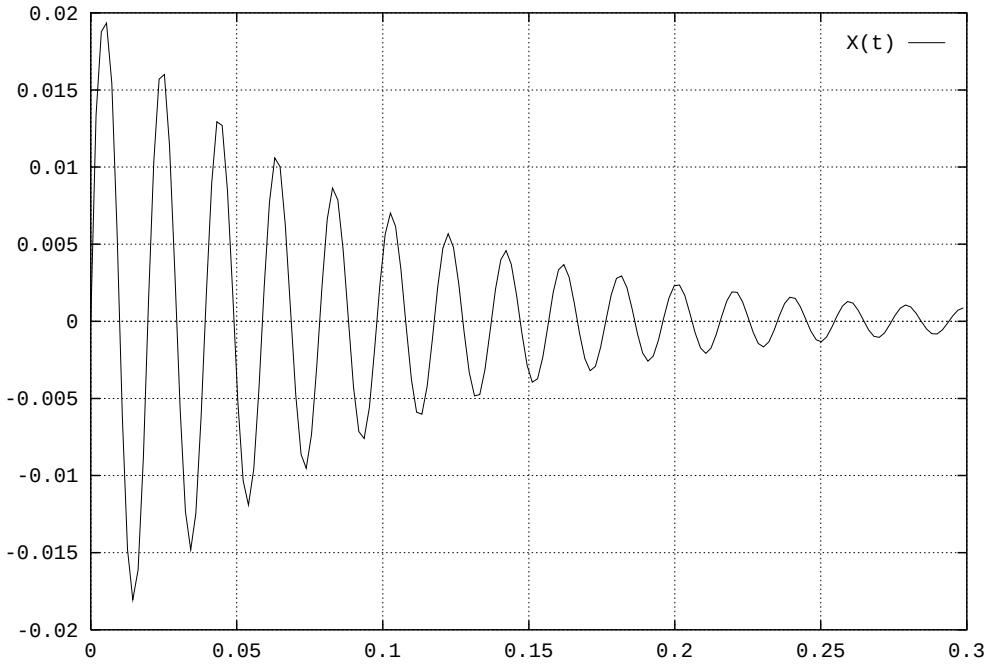

Figure 16: $X(t)$ for the piston problem, **case 1**, $IPC = 2$ and $\Delta t_s = 1.8 * 10^{-3}$

Figure 17. The solution is a little more damped, maybe because we have only 25 time steps per coupled period instead of 100 as in Figure 15. For this method, with $IPC = 2$, unstability does not appear before $\Delta t_s = 8. * 10^{-3}$, which corresponds to 10 time steps per period and $N = 285$, as shown on Figure 18.

Our conclusion is the following. We have tried to increase the stability domain of our method by repeated prediction cycles. This was done successfully, but we got some overdamped solutions when we used too few time steps per coupled period of oscillations. However, we noticed that the predictor for the structural displacement at the end of the current time step was depending on the step ordinal *ipc*. More precisely, there is a slow and oscillating convergence towards a limit. This remark is the starting point for our next prediction method.

5.3.4 Assumed convergence of prediction iterations

The basic idea of this method is the same as peviously. We intend to perform prediction cycles. We have noticed, that for a number of prediction cycles greater than one, the computational cost for the fluid part is at least doubled, for any time step Δt_s. Our goal is to cut down this computational cost. An efficient way would be the following method: for every other P time steps Δt_s, perform actually two prediction cycles. For other time steps, use some information and perform only one cycle with a more efficient prediction. However, this is a little bit idealistic. Indeed, we first try to perform something easier. We first answer the following question: is there a simple way to enhance the performance of the method with $IPC = 2$? For each time step, we lose information, which is the difference between our first prediction,

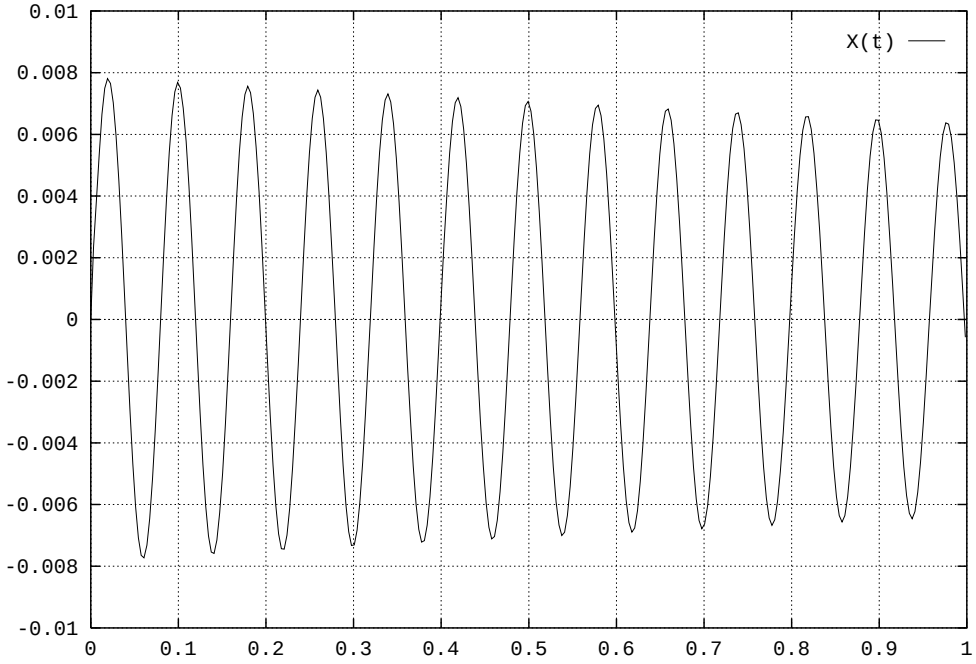

Figure 17: $X(t)$ for the box problem, **case 2**, $IPC = 2$ and $\Delta t_s = 3.2 * 10^{-3}$

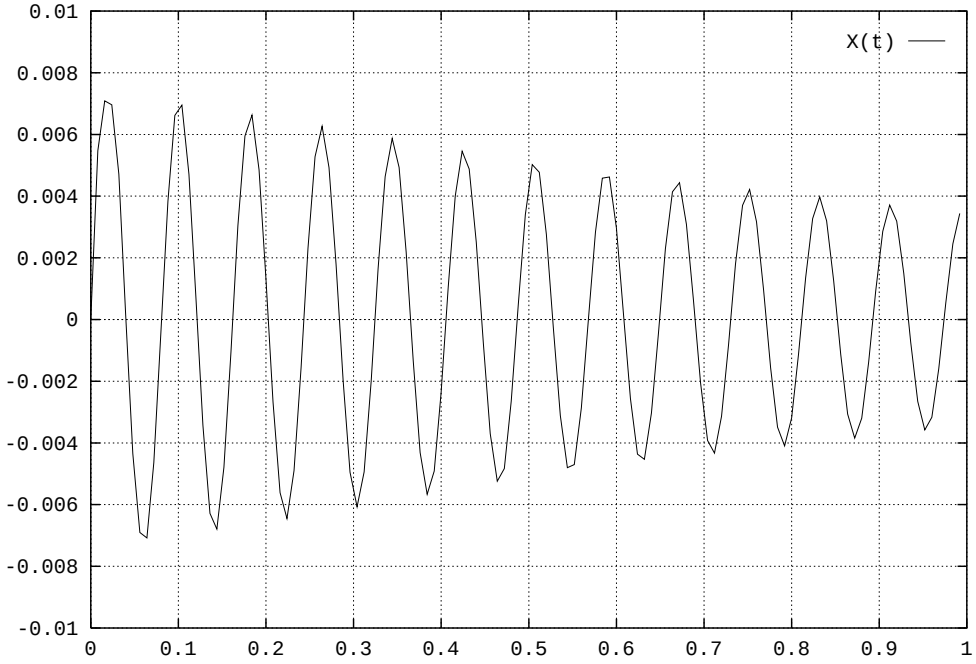

Figure 18: $X(t)$ for the box problem, **case 2**, $IPC = 2$ and $\Delta t_s = 8. * 10^{-3}$

and the final displacement of the structure.

For each prediction cycle, we use a prediction $\widetilde{X^{n+1}}$ for the structural displacement at the end of the current time step in step **2**, and we get a displacement X^{n+1} in step **3**. Then X^{n+1} is a function of $\widetilde{X^{n+1}}$. We make the assumption that this function is linear, i.e.

$$X^{n+1} = -\mathbf{a}^{n+1}\widetilde{X^{n+1}} + \mathbf{b}^{n+1}. \tag{60}$$

where $\mathbf{a}^{n+1}$ and $\mathbf{b}^{n+1}$ are some step dependant coefficients. We know that, for the preceding method, stability increases with the number of prediction cycles. We also know that for an infinite number of prediction cycles, when convergence is achieved, we have $X^{n+1} = \widetilde{X^{n+1}}$, and according to (56) the global energy of the system is conserved. We deduce the following method:

- for the first prediction cycle, use the predictor (57). We write $\widetilde{X^{n+1}}^1$ for this first prediction. We get the structural displacement $\overline{X^{n+1}}$ after the first prediction cycle.
- for the second cycle: compute the value of $\mathbf{b}^{n+1}$ assuming $\mathbf{a}$ is constant by

$$\mathbf{b}^{n+1} = \overline{X^{n+1}} + \mathbf{a}^n \widetilde{X^{n+1}}^1 \tag{61}$$

and use as the second prediction $\widetilde{X^{n+1}}^2$ the fixed point of the the function defined by coefficients $\mathbf{a}^n$ and $\mathbf{b}^{n+1}$, which writes

$$\widetilde{X^{n+1}}^2 = \frac{\mathbf{b}^{n+1}}{1+\mathbf{a}^n}. \tag{62}$$

Finally, since we have computed two evaluations of our assumed linear function, we can update both coefficients in order to satisfy the system

$$\left\{ \begin{array}{rcl} \overline{X^{n+1}} & = & -\mathbf{a}^{n+1}\widetilde{X^{n+1}}^1 + \mathbf{b}^{n+1} \\ X^{n+1} & = & -\mathbf{a}^{n+1}\widetilde{X^{n+1}}^2 + \mathbf{b}^{n+1} \end{array} \right. \tag{63}$$

We present on Figure 19 the results of this method for the piston problem in **case 1**. We show the structural displacements for a time step $\Delta t_s = 1.8 * 10^{-3}$ for this assumed convergence method and for the simple prediction iteration method (Figure 16). The result is less damped and the coupled pulsation is more accurately approximated ($332 s^{-1}$ instead of $317 s^{-1}$, the exact value being $344 s^{-1}$). We show on Figure 20 the corresponding results for $\Delta t_s = 0.9 * 10^{-3}$. Both results are really close. However, though the coupled pulsation is correctly simulated, both solutions are quite overdamped.

We conclude that the errors of the simple prediction iterations method were not corrected by our assumed convergence approach. The method produces disappointing results, and gives no hope about its ability to reduce computational costs, by reducing the proportion of time steps where actual prediction iterations are made as stated at the beginning of this section. This method is elementary. We investigate in the following section the use of numerical filters, which may be well fitted to the natural flexibility of the volume-discontinuous method.

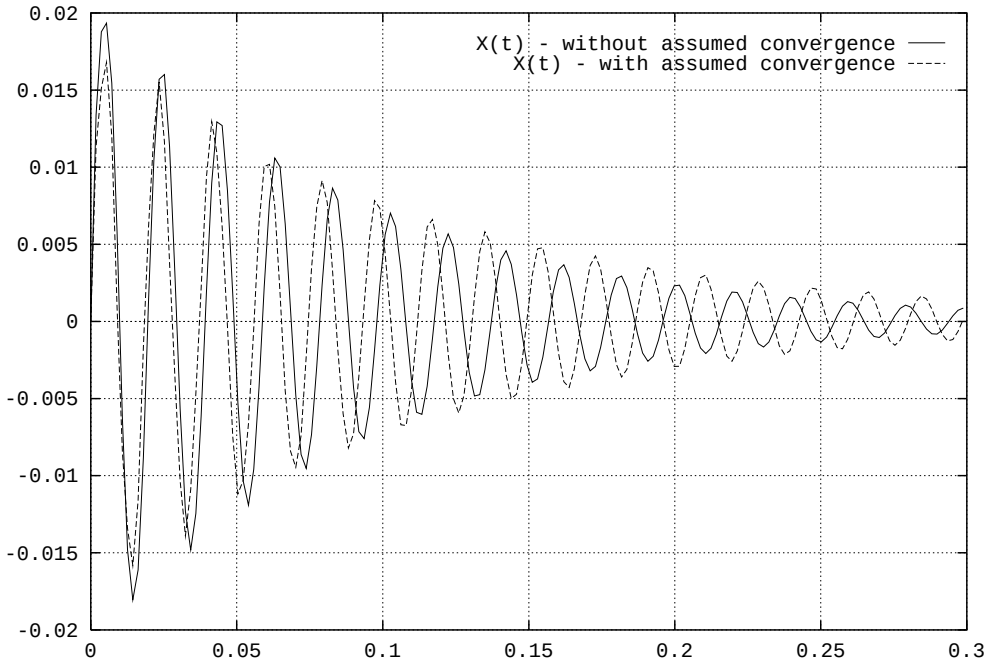

Figure 19: $X(t)$ for the piston problem, **case 1**, $IPC = 2$ and $\Delta t_s = 1.8 * 10^{-3}$

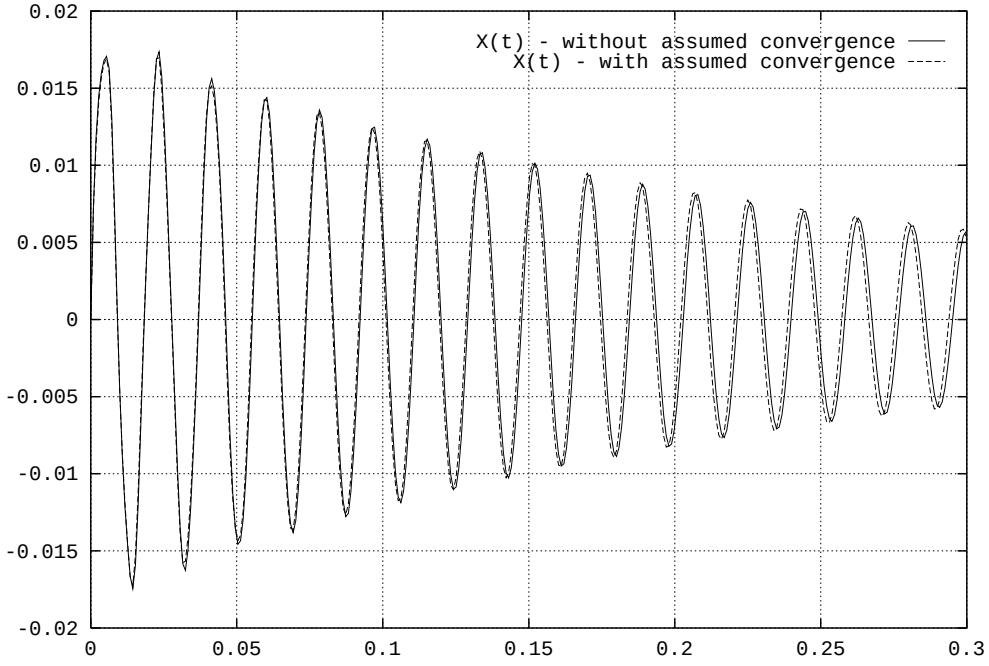

Figure 20: $X(t)$ for the piston problem, **case 1**, $IPC = 2$ and $\Delta t_s = 0.9 * 10^{-3}$

5.3.5 Predictions using filters

If we observe numerical results presented on Figures 6-10-12, we notice that the unstability is first met by some high-frequency mode, that we could call a grid mode. As stated earlier, the volume-discontinuous method has great flexibility. We can use a smoothing prediction for the structural displacement, without applying this smoothing procedure directly to the structure, which could not have been possible with the volume-continuous method.

In order to conserve the generality of the algorithm, we base a new method on adaptive numerical filters, which are able to detect and filter some modes, without defining *a priori* the frequency. In the following, we quickly present adaptive numerical filters, and show their use to provide smooth predictions in our model problems.

Looking at Figure 12, we see that our prediction carries an increasing amount of noise. The transformation of this prediction into something smoother is a typical task of signal processing. Throughout the computation, the prediction (57) gives successive values, which are seen as a signal. A nice course on signal processing can be found in [21]. We are interested in the suppression of high-frequency modes in our incoming signal, and this can be done with numerical filters [22]. However, though we know the structural eigenfrequency, we do not assume we know the coupled eigenfrequency of the system. Then, we have to use adaptive numerical filters, which are able to detect and filter low-frequency modes [23].

In this work, we have used gradient-type adaptive numerical filters. We present now their very simple principle. Let us assume we dispose of a mono-dimensional signal we would like to filter, because we know it is the sum of a sinusoidal signal and a "white" noise (denoted by ϵ), for example

$$x^n = \sin(n\omega_c \Delta t_s) + \epsilon^n \tag{64}$$

For a sinusoidal signal, second order adaptive filters (depending on the two previous data x^n and x^{n-1}) are well fitted because of the following remark:

$$\epsilon^n \equiv 0 \Longrightarrow x^{n+1} - 2\cos(\omega_c \Delta t_s)\, x^n + x^{n-1} \equiv 0 \tag{65}$$

The idea of gradient-type adaptive filters is to consider the left term of the preceding equation as an error on the signal, since it only depends on the noise sequence ϵ. The algorithm is the following:

$$\left\{ \begin{array}{rcl} e^{n+1} & = & x^{n+1} - a_1^n x^n - a_2^n x^{n-1} \\ \\ \left[\begin{array}{c} a_1^{n+1} \\ a_2^{n+1} \end{array} \right] & = & \left[\begin{array}{c} a_1^n \\ a_2^n \end{array} \right] + \delta \left[\begin{array}{c} x^n \\ x^{n-1} \end{array} \right] e^{n+1} \end{array} \right. \tag{66}$$

The reader should notice that the algorithm depends only on a user-fixed parameter δ. No approximation of the term $\omega_c \Delta t_s$ is used. We will see in the following how the parameter δ is fixed.

The result sequence e^n is an approximation of the noise sequence ϵ^n. If we dispose of the input sequence x^n, the output filtered sequence will be $x^n - e^n$. The stability of the algorithm is approximately proved under the assumption that the error e^{n+1} has no correlation with the previous input data (which is fairly true at convergence). Then, stability is achieved when the *a posteriori* error $x^{n+1} - a_1^{n+1} x^n - a_2^{n+1} x^{n-1}$ has a smaller expected value than the *a priori* error $x^{n+1} - a_1^n x^n - a_2^n x^{n-1}$. Thus, we have stability when

$$\delta \sigma^2 < 1 \tag{67}$$

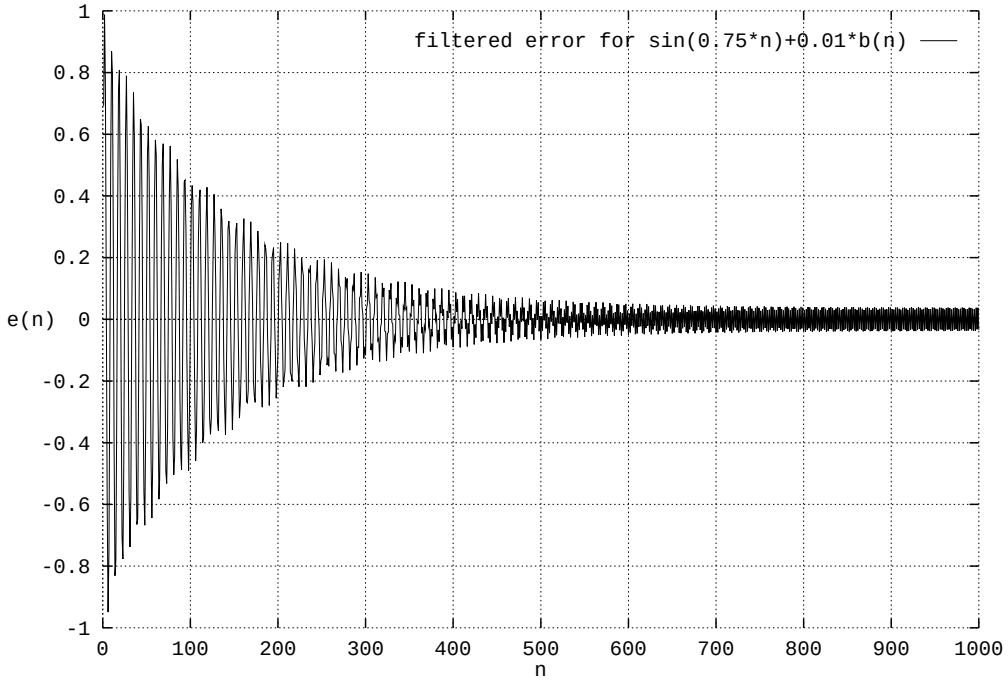

Figure 21: *a priori* error for $x^n = \sin(0.75 * n) + 0.01 * \epsilon^n$ ($\delta = 0.05$)

where δ is the parameter used in (66) and σ^2 is the squared magnitude of the input noise sequence ϵ^n. Usually, the parameter δ is set far below the limit defined by (67), because convergence of sequences a_1 and a_2 might be achieved quicker [23]. We show on Figure 21 the *a priori* error sequence e^n for a typical numerical test (the noise has a unity squared magnitude and we used $\delta = 0.05$).

These filtering methods were coupled to our volume-discontinuous method in the prediction part of our algorithm (the first step; see page 21). The multiple steps of the method can be desdcribed as follows:

- the input for the method is the sequence of piston displacements X^n. When unstability is reached for the simple volume-discontinuous method, we assume some numerical noise increases. We want to get rid of this noise.

- we compute the sequence $Y^{n+1} = X^{n+1} - 2X^n + X^{n-1}$. The high-frequency noise (see for example Figure 14) will be smoothed, and the modulus of X^n is used for the evaluation of the squared magnitude response of Y^n. Actually, the parameter δ is fixed according to $\delta = \frac{1}{12\sigma^2}$ where σ is the sliding maximum of X^n. Coefficients a_1 and a_2 for the sequence Y^n are deduced from the filtering.

- these elements could be sufficient to provide a prediction for the next value of Y, and then for X. However, a general characteristic of the gradient adaptive scheme presented in (66) is that it is not efficient for a typical signal (64) when the parameter $\omega_c \Delta t_s$ is too small. Thus, we filter a subsequence of Y in order to obtain a greater accuracy on the signal Y, and its parameters ($\omega_c \Delta t_s$ and the possible damping). In that step, we have to

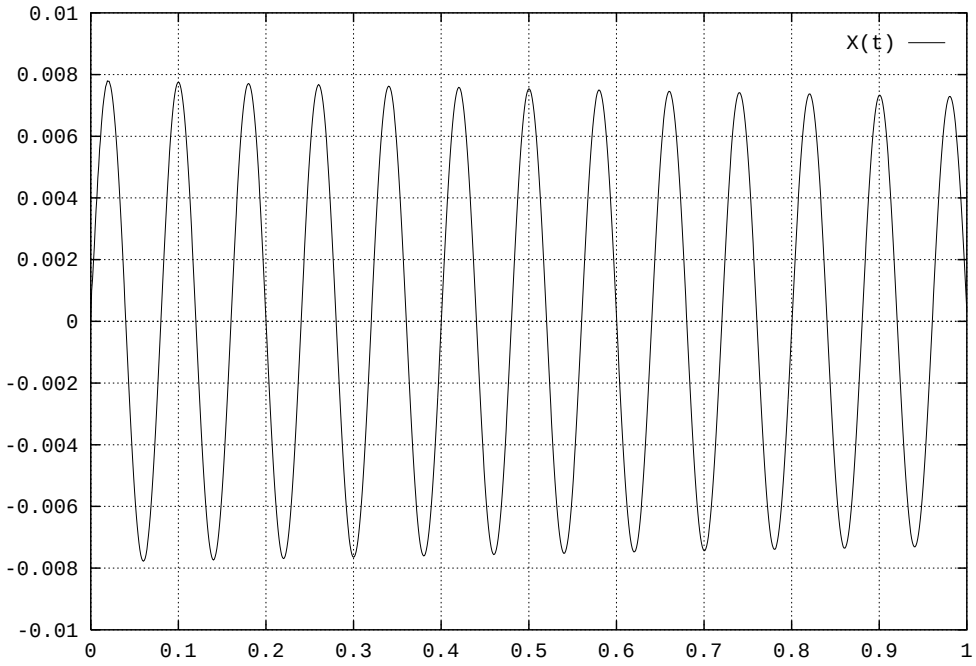

Figure 22: $X(t)$ for the box problem, **case 2**, $\Delta t_s = 1.0 * 10^{-3}$

give an estimate for the coupled pulsation of the system. We use the structural lowest eigenpulsation, and this is the only problem dependant parameter in the method.

- finally, a prediction of X^{n+1} is computed using the assumption that it is the real part of a complex exponential function of the time (or equivalently, of n).

We now present some results for the box problems in **case 2**. We show on Figure 22 the structural displacement for a time step $\Delta t_s = 10^{-3}$ and $N = 36$ (which is to be compared to Figure 12). The method is stable, and produces a very weak numerical damping. A result with $\Delta t_s = 3.2 * 10^{-3}$ and $N = 116$ is presented on Figure 23. In comparison with Figure 17, the result is very satisfying, since the coupled pulsation and the damping numerically observed are very close to those of Figure 17, but the cost of the simulation and the computational storage have been halved.

As a conclusion, we can say that the flexibility of the volume-discontinuous method can be and has been well used. With more or less complex predictions, we have been able to enhance subcycling stability to a satisfying point, since for the case of Figure 23, we have used approximately twenty time steps per coupled period of oscillation, which is a reasonable limit. We would like to put again the emphasis on the fact that the use of the set of predictions presented should not be used for the volume-continuous method, since it would directly affect the structural displacement.

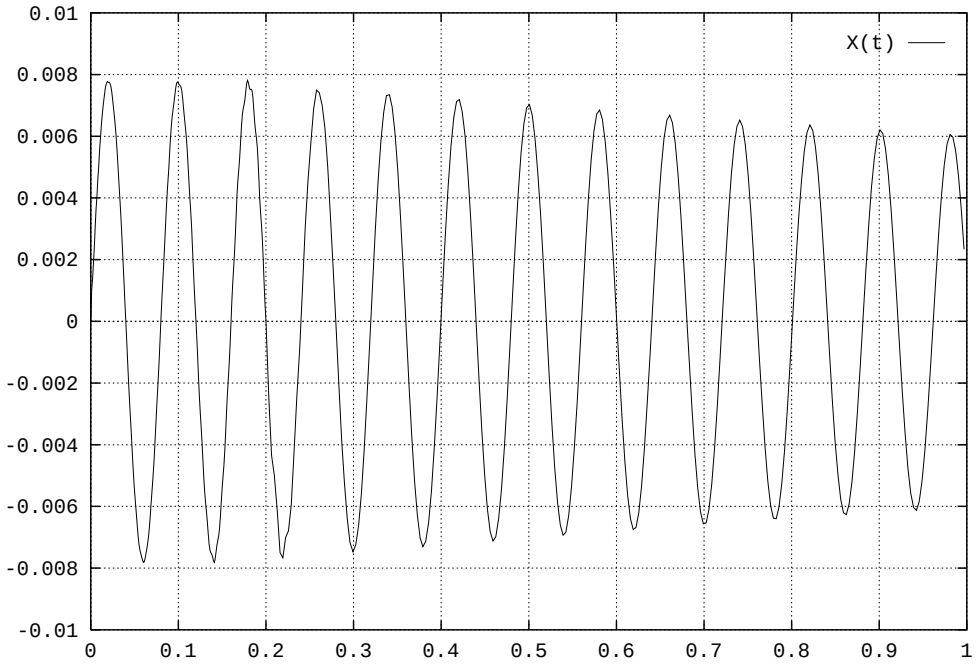

Figure 23: $X(t)$ for the box problem, **case 2**, $\Delta t_s = 3.2 * 10^{-3}$

6 Discussion

In this section, we intend to discuss the possibilities of enhancements of the previous methods and their possible extensions to multi-dimensional aeroelastic problems. We first present some time-interpolation aspects for the previous methods. Then we consider the space-interpolation difficulties that may be encountered for multi-dimensional extensions.

As stated earlier, we have considered subcycled schemes in sections 4 and 5 where the time variation of the fluid mesh was given by (40). This method is not accurate, particularly when the structural time step Δt_s increases. Thus, we first investigate in the following the influence of the time interpolation of the fluid grid motion on the numerical results. Throughout this paper, we have used the linear law of motion (40)for the fluid mesh during subcycles. This law of motion could be more accurate. However, in most cases, like computations corresponding to Figures 18-20, we tried with no success to reduce numerical damping. Actually, the numerical damping was caused by the use of a big structural time step Δt_s, which gave us a quite unaccurate prediction for the structural displacement at the end of the step. The unaccuracy of the linear motion of the fluid mesh was covered by the unaccuracy of the prediction.

However, some work has been done on time-interpolation aspects in cases where we disposed of a very accurate prediction of the structural displacement. For example, adaptive numerical filtering produces as an output informations on the pulsation and phase of the processed signal. These informations can be easily used to construct some accurate law of motion for the fluid mesh. This was done successfully, as shown on Figure 24, which presents another result for the same test case as Figure 23.

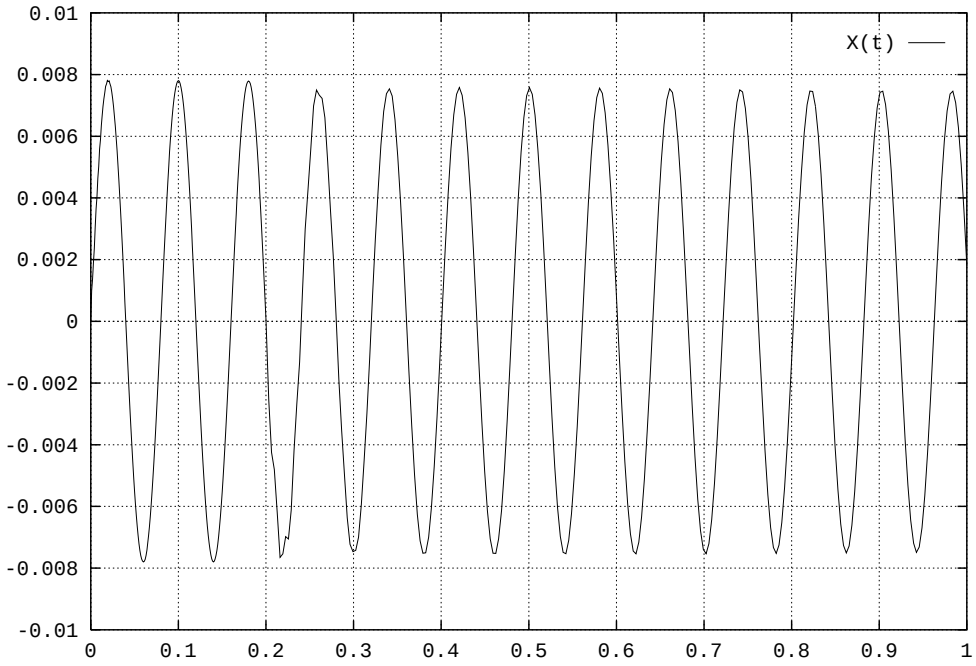

Figure 24: $X(t)$ for the box problem, **case 2**, $\Delta t_s = 3.2 * 10^{-3}$ (non-linear mesh motion)

The structural displacement is very slightly damped. This damping was produced by the numerical viscosity added in the fluid by the explicit first-order numerical scheme. The preceding result is quite optimal, since damping and pulsation are well simulated, and stability is conserved though $\omega_c \Delta t_s = 0.25$ (which corresponds to 25 time steps per coupled period of oscillations).

We also tested the generalized-α method we presented in (21-23). This method was constructed to control and possibly reduce high-frequency modes by using a user-specified high-frequency dissipation. However, the generalized-α method is used for the structure only. In the test cases we considered in this paper, the structure is reduced to a point and the only eigenfrequency is low. Then the generalized-α method may not have any influence on high-frequency coupled modes. This was numerically confirmed. The generalized-α method will be used in future works for complex structures.

As said before, our structure is reduced to a material point (one degree of freedom). We then have not mentionned any spatial interpolation problem at the fluid/structure interface. This might be the least straightforward part of the extension of the methods to multi-dimensional cases. In the case where the fluid and the structural meshes are conforming (same vertices at the common interface), the extension of the volume-continuous method is easy. For the volume-discontinuous method, and for the volume-continuous method when both grids are not conforming, the extension is a little more complex. Both methods should be added a procedure allowing the transfer of pressure forces and structural displacements between the fluid and the structure. Because the most part of industrial test cases are non-conforming - usually, fluid and structural spatial discretizations are different - this kind of procedure has already been implemented (see [20] for example).

We will focus our future work on the extension of the methods presented in this paper to two-dimensional problems, and particularly, to the Euler flutter analysis of a classical NACA airfoil, first with two and then with a great number of degrees of freedom. Our aim will be the use of subcycling schemes, which allow a limited number of structural time-integrations (optimal would be twenty-five like the box problem seen previously) per coupled period of oscillations.

ACKNOWLEDGEMENTS:
We wish to thank our colleagues Charbel Fahrat and Nathan Maman (both at the Center for Space Structures and Control, University of Colorado at Boulder), and Stéphane Lantéri (INRIA Sophia-Antipolis) for their impressive support and help, and for the expensive time they massively devoted to fruitful discussions on numerical simulation of fluid/structure interactions.

References

[1] S. Piperno. Numerical methods used in aeroelasticity simulations. *Rapport de Recherche CERMICS*, 92-5, 1992.

[2] R.D. Rausch, J.T. Batina, and H.T.Y. Yang. Euler flutter analysis of airfoils using unstructured dynamic meshes. AIAA paper 89-1384, April 3-5 1989. AIAA/ASME/ASCE/AHS/-ASC 30th Structures, Structural Dynamics and Materials Conference, Mobile, Alabama.

[3] S. Piperno, C. Farhat, and B. Larrouturou. Partitioned procedures for the transient solution of coupled aeroelastic problems. Center for Aerospace Structures - 94-06, University of Colorado, Boulder, Colorado, January 1994.

[4] K.C. Park, C.A. Felippa, and J.A. De Runtz. Stabilization of staggered solution procedures for fluid-structure interaction analysis. In T. Belytschko and T.L. Geers, editors, *Computational methods for fluid-structure interaction problems*, pages 26.94–26.124. ASME Applied Mechanics Symposia Series, 1977.

[5] S. Piperno, B. Larrouturou, and M. Lesoinne. Analysis and compensation of numerical damping in a one-dimensional aeroelastic problem. *Rapport de Recherche CERMICS*, 93-17, 1993.

[6] C. Farhat and T.Y. Lin. Transient aeroelastic computations using multiple moving frames of reference. AIAA paper 90-3053-CP, 1990.

[7] S. Lanteri and C. Farhat. Rapport de recherche aéroélasticité. deuxième partie : étude bibliographique et analyse des méthodes. Contrat DRET/AMDBA/PGSoft/INRIA, 1992.

[8] J. Chung and G.M. Hulbert. A time integration algorithm for structural dynamics with improved numerical dissipation: the generalized-α method. *Transctions of ASME, Journal of Applied Mechanics*, 60:371–375, June 1993.

[9] S. Lanteri and C. Farhat. Rapport de recherche aéroélasticité. première partie : étude bibliographique. Contrat DRET/AMDBA/PGSoft/INRIA, 1992.

[10] T.J.R. Hughes and W.K. Liu. Implicit-explicit finite elements in transient analysis: stability theory. *Transactions of the ASME, Journal of Applied Mechanics*, 45:371–374, June 1978.

[11] H.M. Hilber, T.J.R. Hughes, and R.L. Taylor. Improved numerical dissipation for time integration algorithms in structural dynamics. *Earthquake Engineering and Structural Dynamics*, 5:283–292, 1977.

[12] W.L. Wood, M. Bossak, and O.C. Zienkiewicz. An alpha modification of newmark's method. *International Journal for Numerical Methods in Engineering*, 15:1562–1566, 1981.

[13] J. Donea, S. Giuliani, and J.P. Halleux. An arbitrary lagrangian eulerian finite element method for transient dynamic fluid-structure interactions. *Computer Methods in Applied Mechanics and Engineering*, 33:689–723, 1982.

[14] B. Van Leer. Flux-vector splitting for the euler equations. *Lecture Notes in Physics*, 170:pp 507–512, 1982.

[15] J.T. Batina. Implicit flux-split euler schemes for unsteady aerodynamic analysis involving unstructured dynamic meshes. *AAIA Journal*, 29:1836–1843, Nov 1991.

[16] B. N'Konga and H. Guillard. Godunov type method on non-structured meshes for three-dimensional moving boundary problems. INRIA RR-1883, INRIA Sophia-Antipolis, Avril 1993.

[17] W.K. Anderson, J.L. Thomas, and C.L. Rumsey. Extension and application to unsteady calculations on dynamic meshes. *AIAA Journal*, 27(6):673–674, June 1989.

[18] M. Lesoinne and C. Farhat. Stability analysis of dynamic meshes for transient aeroelastic computations. In *11th AIAA Computational Fluid Dynamics Conference, Orlando, Florida*, July 6-9 1993. AIAA paper 93-3325.

[19] J.T. Batina. Unsteady euler airfoil solutions using unstructured dynamic meshes. *AIAA Journal*, 28:1381–1388, Aug 1990.

[20] N. Maman and C. Farhat. Matching fluid and structure meshes for aeroelastic computations: a parallel approach. Center for Aerospace Structures - 93-12, University of Colorado, Boulder, Colorado, June 1993.

[21] M. Bellanger. *Traitement numérique du signal.* CNET-ENST, Collection technique et scientifique des télécommications. Masson, 1987.

[22] R. Boite and H. Leich. *Les filtres numériques.* CNET-ENST, Collection technique et scientifique des télécommunications. Masson, 1990.

[23] M. Bellanger. *Analyse des signaux et filtrage numérique adaptatif.* CNET-ENST, Collection technique et scientifique des télécommunications. Masson, 1989.

Contents

Liste des derniers rapports de recherche du CERMICS

List of previous CERMICS research reports

93-17	S. Piperno, B. Larrouturou et M. Lesoinne	*Analysis and Compensation of Numerical Damping in a one-dimensional Aeroelastic Problem*, 31 pages, juin 1993, Sophia-Antipolis
93-18	G. Caplain, R. Lalement et T. Salset	*Semantic analysis of a control-parallel extension of Fortran*, 46 pages, juin 1993, Noisy-le-Grand
93-19	M. Loriot and L. Fezoui	*A Parallel Compressible 3D Navier-Stokes Solver Using Unstructured Meshes*, 17 pages, septembre 1993, Sophia-Antipolis
93-20	D. Issautier	*Algorithmes Particulaires pour Calculateurs à Architecture Massivement Parallèle*, 11 pages, octobre 1993, Sophia-Antipolis
93-21	Y. D'Angelo et B. Larrouturou	*Comparison and Analysis of some Numerical Schemes for Stiff Complex Chemistry Problems*, 34 pages, octobre 1993, Sophia-Antipolis
93-22	F. Lebastard	*CHOOE: Un gestionnaire d'environnement distribué*, 27 pages, décembre 1993, Sophia-Antipolis
93-23	L. He et B. Larrouturou	*Moving Grid Numerical Simulations of Planar Time-Dependent Detonations*, 28 pages, décembre 1993, Sophia-Antipolis
94-24	A. Ern, V. Giovangigli	*Multi-Component Transport Algorithms*, 270 pages, janvier 1994, Noisy-le-Grand
94-25	L. Sainsaulieu	*Equilibrium Velocity Distribution Functions for a Kinetic Model of Two-phase Flows*, 22 pages, janvier 1994, Noisy-le-Grand

94-26	R. Carpentier, A. de la Bourdonnaye B. Larrouturou	*On the Derivation of the Modified Equation for the Analysis of Linear Numerical Methods*, 14 pages, janvier 1994, Sophia-Antipolis
94-27	P.A. Raviart, L. Sainsaulieu	*A Nonconservative Hyperbolic System Modeling Spray Dynamics. Part 1. Solution of the Riemann Problem*, 37 pages, avril 1994, Noisy-le-Grand
94-28	E. Burman, L. Sainsaulieu	*Numerical Analysis of Two Operator Splitting Methods for an Hyperbolic System of Conservation Laws with Stiff Relaxations Terms*, 32 pages, avril 1994, Noisy-le-Grand
94-29	G. Caplain	*Correctness properties in a control-parallel extension of Fortran*, 27 pages, septembre 1994, Noisy-le-Grand
94-30	F. Berreux, L. Sainsaulieu	*A Roe-type Riemann solver for hyperbolic systems with relaxation, based on time-dependent wave decomposition*, 48 pages, novembre 1994, Noisy-le-Grand
94-31	L. Sainsaulieu	*Traveling waves solution of convection-diffusion systems whose convection terms are weakly non conservative. Application to the modeling of two phase fluid flows*, 31 pages, novembre 1994, Noisy-le-Grand
94-32	M. Bouzoubaa	*Houria : un résolveur de système de contraintes fonctionnelles hiérarchique*, 18 pages, novembre 1994, Sophia-Antipolis
94-33	S. Piperno	*Méthodes d'intégration temporelle décalée pour un problème aéroélastique mono-dimensionnel non linéaire*, 42 pages, décembre 1994, Sophia-Antipolis

Ces rapports peuvent être obtenus en s'adressant aux secrétariats du CERMICS :
The reports can be asked from:

Monique Razurel
CERMICS-ENPC
F–93167 Noisy-le-Grand CEDEX
Tél : (33) 1 - 43 04 40 98
email: `razurel@enpc.fr`

Hélène Evin
CERMICS-INRIA
B.P.93
F–06902 Sophia-Antipolis Cedex
Tél : (33) 93 65 79 00
email: `hevin@sophia.inria.fr`